SEDIMENTOLOGY the journal of the International Association of Sedimentologists

Sedimentology (2023) doi: 10.1111/sed.13129

Spatial distribution and variability of lobe facies in a large sand-rich submarine fan system: Neoproterozoic Zerrissene Group, Namibia

NORA M. NIEMINSKI*, TIM R. MCHARGUE†, JARED T. GOOLEY‡, ANDREA FILDANI§ and DONALD R. LOWE†

**U.S. Geological Survey, Pacific Coastal and Marine Science Center, Santa Cruz, CA 95060, USA (E-mail: norski.geo@gmail.com)*

†Department of Geological Sciences, Stanford University, Stanford, CA 94305, USA

‡U.S. Geological Survey, Alaska Science Center, Anchorage, AK 99508, USA

§The Deep Time Institute, Danville, CA 94526, USA

Associate Editor – Jeff Peakall

ABSTRACT

The deposits of the upper Neoproterozoic Zerrissene Group of central-western Namibia represent a large siliciclastic deep-water depositional system that showcases the intricacies of facies and architectural relationships from bed-scale to fan-system-scale. The lack of vegetation in the Namib Desert and regular east–west repetition of folded stratigraphy (reflecting *ca* 50% tectonic shortening) provides quasi-three-dimensional exposure over a current area of approximately 2700 square kilometres. The Brak River Formation, the middle sand-rich unit of the Zerrissene Group, consists of nearly 600 m of strata exposed in multiple parallel continuous outcrops up to *ca* 10 km in length and oriented obliquely to depositional dip. Ten stratigraphic sections are correlated *ca* 32 km (*ca* 64 km restored) across the basin and offer exposure comparable in scale to modern submarine fans. Six sedimentary facies are identified and grouped into four facies associations that represent axial-to-marginal portions of deep-water lobes in an unconfined submarine fan system. Spatial facies patterns, regional thickness variations, and palaeocurrents indicate that Brak River Formation sediments were transported primarily from the north to south–south-west through a trough-like basin, and deposited within an unconfined basin plain at the junction of the Adamastor and Khomas oceans. The unique outcrop exposure and extent permits the documentation of system-scale architecture and basin configuration of the Brak River submarine fan system. A transition from the sand-rich lower Brak River Formation to more intercalated mudstone-dominated intervals in the middle and upper Brak River Formation is interpreted to record a change from aggradational to compensational stacking of lobe deposits. This records the evolution of a large submarine fan as it filled the subtle seafloor topography and became less confined at the system-scale. The documentation of these deep-water deposits from centimetre-scale to basin-scale provides a new model for a system with extensive long-distance transport of sand-rich sediment gravity flows to submarine lobes without apparent channelization.

Keywords Compensational stacking, deep-water lobe deposits, glaciogenic, Neoproterozoic, stratigraphic architecture, submarine fan, transitional flow deposits, turbidites.

INTRODUCTION

The spatial variability of deep-water sedimentary facies can reveal information about sediment gravity flow processes and the resulting distribution of their deposits. Deep-water processes can be efficient at delivering large amounts of detritus (e.g. Talling *et al.*, 2007), nutrients, and pollutants (e.g. Kane & Fildani, 2021) into the deepest reaches of the modern oceans. Thus, large deep-water fans provide an archive of oceanic, continental, and climatic records (Hessler & Fildani, 2019). Located at the termini of continental-scale drainages, deep-water fan deposits offer a comprehensive stratigraphic record that preserves environmental and sedimentary signals that can inform us about tectonic and plate boundary configurations (e.g. Clift *et al.*, 2008; Sharman *et al.*, 2013; Gooley *et al.*, 2021), major perturbations in climate (e.g. Prins & Postma, 2000; Mason *et al.*, 2019), changes in sea level (e.g. Weber *et al.*, 1997; Covault *et al.*, 2007), drainage reorganization of continental-scale rivers (e.g. Sharman *et al.*, 2017; Fildani *et al.*, 2018a), and even past earthquake records (e.g. Goldfinger *et al.*, 2003; Polonia *et al.*, 2017).

While unconfined submarine fan deposits can be vast, on the order of tens to hundreds of kilometres in scale, studies of these systems are often challenged by relatively poor preservation and limited extent of outcrop exposures, insufficient resolution in available seismic reflection data, and limited accessibility to modern examples. Outcrop exposures of unconfined fans have been documented (for example, Neoproterozoic Kaza Group of the Windermere Supergroup, Upper Carboniferous Ross Formation and Permian Skoorsteenberg Formation; *cf.* Prélat *et al.*, 2009; Terlaky *et al.*, 2016; Martinsen *et al.*, 2017), but investigations into spatial variability of deep-water facies on a fan system scale are limited due to size and relative paucity of outcrops that expose the entirety of large, sand-rich unconfined turbidite systems. Thus, current models and our basic understanding of such systems are largely based on composites of smaller outcrops and, more recently, from high-resolution studies of modern systems (e.g. Lopez, 2001; Carvajal *et al.*, 2017; Fildani *et al.*, 2018b; Maier *et al.*, 2020). The complexity of facies distributions in large, unconfined submarine fans leads to challenges in predicting the geometries of their deposits. Thus, there is an increasing need for outcrop analogues of such deep-water systems in order to understand the facies distributions of analogous subsurface exploration targets (e.g. Chapin, 1998; Zarra, 2007) or, alternatively, as CO_2 storage reservoirs (e.g. Ketzer *et al.*, 2005).

To more adequately address the architecture and lateral facies relationships of deep-water lobe deposits, outcrop continuity that surpasses the scale of lobes within a submarine fan system is needed. The Neoproterozoic Zerrissene turbidite system in central-western Namibia is a well-exposed, continuous succession of one of the largest turbidite systems preserved in outcrop (Miller *et al.*, 1983a; Swart, 1992). The exposed stratigraphy of the Zerrissene Group is located in the lower Ugab River region and covers an area of roughly 2700 km^2 (Fig. 1A). Given uncertainties in the degree of tectonic shortening, the exposed deposits of the Zerrissene Group may represent up to 5400 km^2 of palaeogeographical area when structurally restored (*ca* 50% east–west shortening), although the shape, size, and configuration of the entire basin has not been determined (Swart, 1992). While these outcrops are among the most laterally extensive exposures of deep-water systems in the world, they are understudied because of their remote location, greenschist-grade metamorphic overprinting, and isoclinal, often recumbent, folding. Despite these complexities, the siliciclastic units of the Zerrissene Group still preserve primary sedimentary structures, and thrust faulting and isoclinal folding provide multiple parallel, laterally extensive cross-sections through the system (Fig. 2). This study aims to improve understanding of sand-rich unconfined turbidity current deposition and provide a large, relatively fine-grained outcrop analogue that can be used to address how depositional processes and sediment characteristics relate to stratigraphic architecture and facies distribution in unconfined deep-water lobe deposits at the scale of the entire fan system. The east–west repetition of Zerrissene Group stratigraphy allows for a quasi-three-dimensional view of the deposits in the context of the whole submarine fan system and offers an ideal setting for documenting unconfined deep-water deposits at: (i) the centimetre-scale to investigate the nature of depositing flows from lobe axis to lobe fringe environments; (ii) metre-scale to understand drivers of lobe stacking patterns and address whether the fringes of sand-rich lobe complexes are resolvable in the stratigraphic record; and (iii)

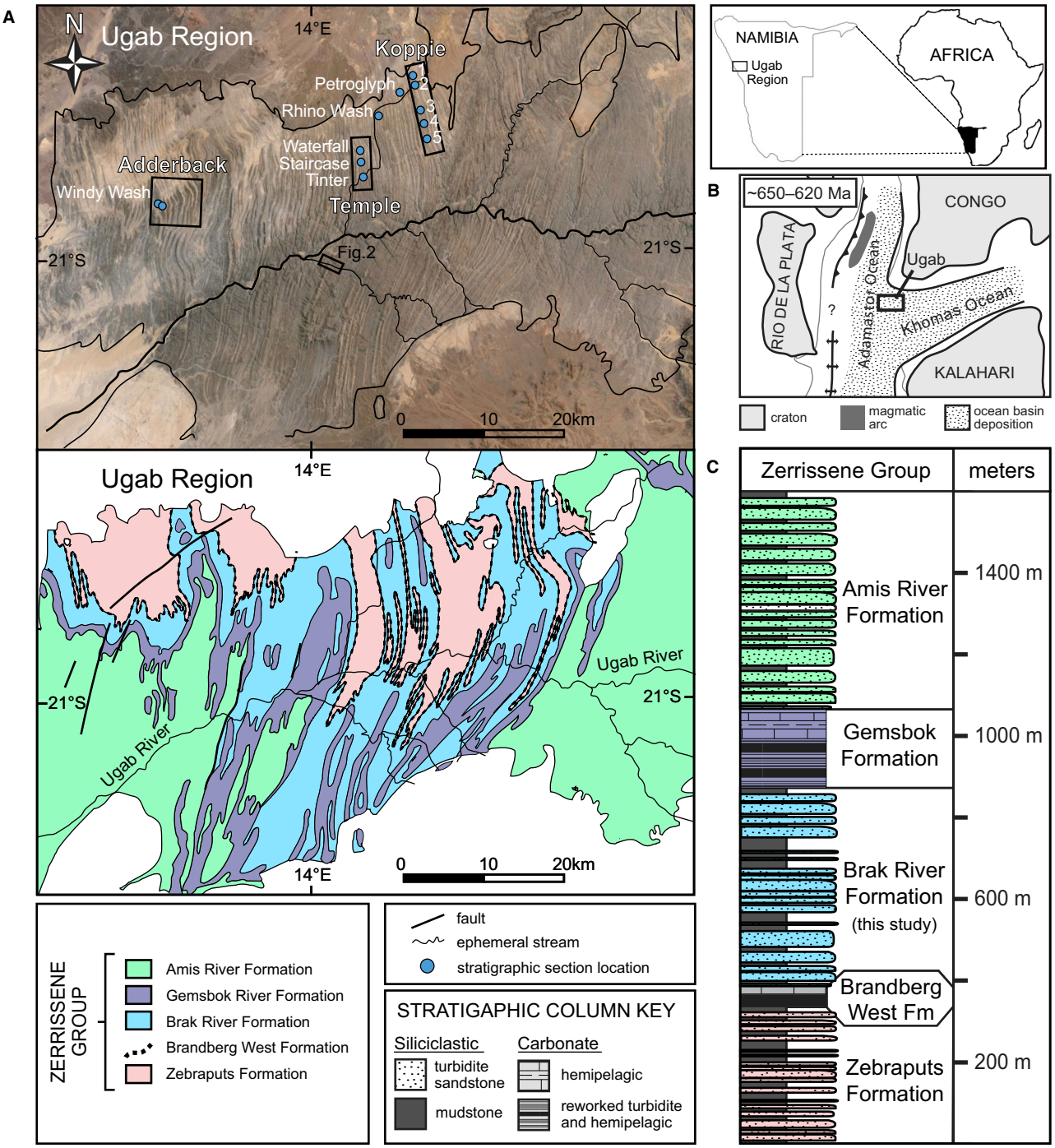

Fig. 1. (A) Satellite image (top) and simplified geological map (bottom) of the Ugab Region study area (after Miller & Schalk, 1980; Swart, 1994) and full exposure of the Zerrissene Group. (B) Regional palaeogeographical reconstruction modified after Nieminski *et al.* (2019) showing the approximate location of the Ugab depocentre at the time of deposition of the Zerrissene Group. (C) Simplified stratigraphic column of the Zerrissene Group. Formation thicknesses are from Swart (1992).

a scale of hundreds of metres to document basin configuration (for example, orientation, seafloor topography, and sediment input), and its observable influence on the lateral and stratigraphic variability of large unconfined fan systems.

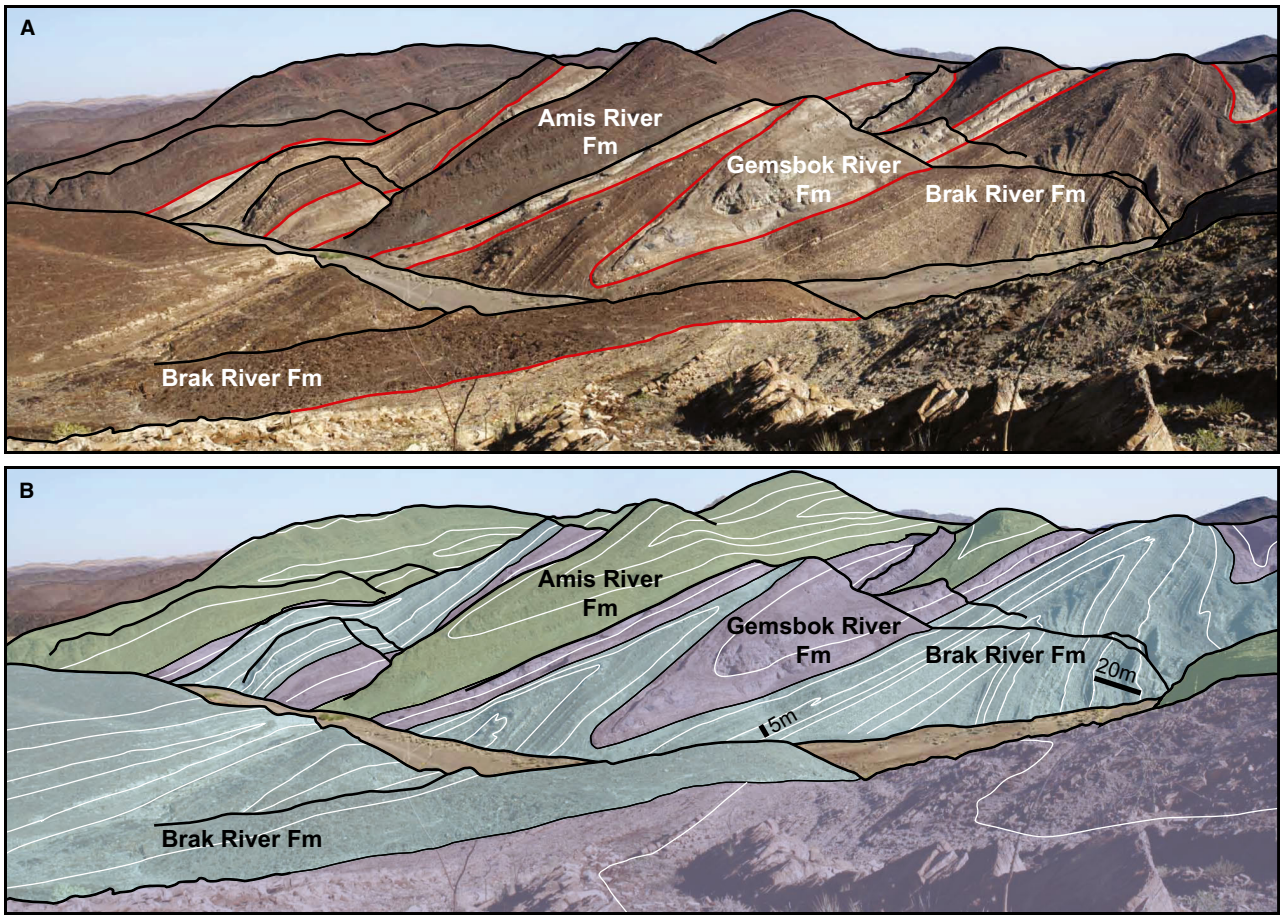

Fig. 2. (A) Tight isoclinal folding of the Zerrissene Group with formation (Fm) contacts highlighted in red and major topography outlined in black. Location is indicated in Fig. 1A. (B) Interpreted photograph highlighting the three uppermost formations of the Zerrissene Group and internal folding of a few traced beds (white lines). Scales are provided on both the relatively undeformed overturned limb and the sheared, thinned upright limb of the Brak River Formation to highlight the pervasive folding in the region. Locations where stratigraphic sections were measured (Fig. 1A) were carefully chosen to avoid this type of particularly tight isoclinal folding.

GEOLOGICAL CONTEXT

The Zerrissene Group comprises three deep-water siliciclastic units intercalated with two marbleized carbonate units (Fig. 1C; Nieminski *et al.*, 2019). Geological work in the Zerrissene region began in the 1940s and subsequently increased with the search for ore deposits in the area (Swart, 1992). The first mapping of the Ugab River region was performed by Jeppe (1952), after which the turbiditic nature of the Zerrissene Group was first recognized by Miller *et al.* (1983a). Age correlations of the Neoproterozoic Zerrissene Group were made with lithostratigraphic and chronostratigraphic markers in the Damara Orogen by Jeppe (1952) and Miller *et al.* (1983b), and are revised and summarized by Nieminski *et al.* (2019) using detrital zircon U–Pb geochronology. Swart (1992) provided a stratigraphic model for the sedimentary evolution of the entire Zerrissene system and a preliminary investigation of the basin's tectonic setting based on petrographic and geochemical analyses.

The Zerrissene turbidites were deposited at the junction of the north–south-trending Adamastor Ocean and the east–west-trending Khomas Ocean, formed between the South American Rio de la Plata Craton and the African Congo and Kalahari cratons (Frimmel *et al.*, 1996; Gray *et al.*, 2006) during early spreading after the continental breakup of Rodinia (Fig. 1B; Miller, 1983; Hoffman *et al.*, 1994; Miller *et al.*, 2009). The Zerrissene Group predominantly received sediment from the Congo Craton and magmatic arc terrane of the Dom

Feliciano Belt of Uruguay and has a maximum depositional age ranging from 662.0 ± 13.6 to 624.5 ± 3.5 Ma for the lowest to uppermost siliciclastic unit, respectively (Nieminski *et al.*, 2019). The depositional age and presence of dropstones in siliciclastics overlain by carbonates suggest that the Zerrissene sediments likely include post-glacial cap carbonates that record the global 'Snowball Earth' Marinoan (*ca* 640 Ma) Glaciation (Hoffman *et al.*, 1998; Halverson *et al.*, 2005, 2007; Nieminski *et al.*, 2019).

The Zerrissene Group was structurally incorporated into the Damara Orogen around 560 to 550 Ma, during the collision of South America with Africa, when the Kalahari Craton and adjacent oceanic crust were subducted beneath the Congo Craton (Coward, 1981; Miller, 1983, 2008; Porada & Wittig, 1983; Kukla & Stannistreet, 1991; Prave, 1996). This orogeny represents one of the many global collisional events that created a worldwide series of mountains during the formation of the Gondwana supercontinent, which is thought to have sutured between 570 and 510 Ma (Meert & Van Der Voo, 1997; Boger *et al.*, 2001; Boger & Miller, 2004; Rapalini, 2006; Tohver *et al.*, 2006; Gray *et al.*, 2008). As a result, the Ugab Region is characterized by tight, north–south-striking, westward-verging asymmetrical overturned folds (Figs 1A and 2) that formed during north-west/south-east transpression and east–west compression (Freyer & Hälbich, 1994; Goscombe *et al.*, 2003; Miller, 2008; Seth *et al.*, 2008; Maeder *et al.*, 2014). Later stage north–south shortening created superimposed undulations in axes of the primary folds (Freyer & Hälbich, 1994; Goscombe *et al.*, 2003).

METHODS

Spatial variation of the Zerrissene system was investigated in the middle siliciclastic Brak River Formation, which has the most continuous and relatively undeformed exposures throughout the study area (Fig. 1). Ten stratigraphic sections (cumulative over 4.8 km of strata) were measured and correlated through the Brak River Formation (Appendix S1). These sections were measured in four separate fold limbs to document any variability in depositional facies across the basin: two adjacent limbs in the locality named Koppie, and one in each of the localities named Temple and Adderback (Fig. 1A). Two of these stratigraphic sections (one at Koppie and one at Adderback) encompass approximately the entire thickness of the Brak River Formation and document how this thickness varies across the basin (*ca* 600 to 900 m). Two additional partial sections (Rhino Wash and Windy Wash) were measured in isolated fold limbs where portions of the Brak River Formation are exceptionally exposed (Fig. 1A; Appendix S2). Palaeocurrent data were collected where available from ripple cross-laminations and sole marks. All palaeocurrent data were corrected for bedding rotation and fold plunge (*ca* 5 to 10°) in Stereonet 8.6.0 (Cardozo & Allmendinger, 2013) and are compiled in Appendix S3.

Stratigraphic sections were measured at the centimetre-scale, but with varying degree of detail regarding sedimentary structures, depending on the locality and quality of the exposure. An architectural hierarchy was defined for the Zerrissene system to better characterize one-dimensional and two-dimensional detail with stratigraphic sections and correlations, respectively (Table 1; Fig. 3). Stratigraphic sections document sedimentary facies and facies associations that were correlated between sections in addition to individual beds that were traced within fold limbs. Correlations between stratigraphic sections within the same fold limb were made at the metre-scale, with the thickest sandstone bed correlations confirmed in the field. Bed correlations that were not walked out in the field, were traced on satellite imagery of each of the fold limbs, as were sedimentary facies. Petrographic thin sections were cut from two samples near the base and top of a sandstone bed representative of one of the sedimentary facies (SF5) to visually assess relative mudstone content. Percent sandstone (sandstone thickness relative to total stratigraphic thickness) was calculated for all of the localities and for each of the 10 measured sections with the purpose of assessing spatial and temporal variation in sand accumulation throughout the basin.

DESCRIPTION OF OUTCROP LOCALITIES

The tight folds in the Ugab Region have highly sheared upright limbs and better-preserved overturned limbs that allow for measuring stratigraphic sections (Fig. 2). Metamorphic deformation is reflected by low-grade, greenschist-facies and high-angle cleavage to bedding. Due to low-grade

Table 1. Zerrissene Group hierarchy in the context of other deep-water lobe system hierarchies.

This study			Prélat *et al.* (2009)		Mulder & Etienne (2010)		Terlaky *et al.* (2016)	
Order	Nomenclature	Thickness (m)	Nomenclature	Thickness (m)	Nomenclature	Thickness (m)	Nomenclature	Thickness (m)
7th	System	>300	–	–	–	–	Fan complex	NA
6th	Lobe Complex set	100–300	Fan	–	Lobe complex	>100	Fan	NA
5th	Lobe Complex	20–100	Lobe complex (fan)	30–60	Lobe system	>20	Lobe complex	NA
4th	Lobe Deposit/ Facies Association	2–20	Lobe	4–10	Lobe	3–9	Lobe	<1–50 (us. 1–35)
3rd	Sedimentary facies	0.5–15	Lobe element (lithofacies)	1–3	Lobe element	1–2	Stratal element	1–10
2nd	Bed	0.01–10	Bed	0.03–10	Lobe bed	0.03–10	Bed	1–9
1st	Bed division	0.01–0.20	–	–	–	–	–	–

metamorphism, grain size is difficult to determine and is approximated in many places. Mudstone is easy to differentiate because it has particularly dense cleavage relative to siltstone and sandstone. Aside from only a few localities, sedimentary structures are obscured by desert varnish and metamorphic overprint. The best exposures available are those exposed along the polished sides of ephemeral stream washes in the study area. The three localities selected for this study expose overturned fold limbs that are polished in places and relatively continuous. The Koppie, Temple, and Adderback localities (Fig. 1A) are described below.

Koppie

Farthest east of the studied localities, the Koppie locality offers the longest uninterrupted lateral exposure of the Brak River Formation in a single fold limb, with 12 km of relatively continuous outcrop (Fig. 4). Previous work in this locality includes that of Lyons *et al.* (2007) that documented several potential pinch-outs (lateral termination) of otherwise continuous 'bundles' of amalgamated sandstone beds and estimated an average bundle thickness of 2.5 m. The observations of Lyons *et al.* (2007) are primarily based on interpreted aerial photographs that were checked in the field along most of the north–south-oriented fold limb.

For this study, five stratigraphic sections (Koppie 1 to 5, from north to south) were measured and field correlated to one another (Fig. 4B). Four of the five sections include the basal contact of the Brak River Formation with the underlying Brandberg West Formation. Due to incomplete exposure of the uppermost sandstone beds within the Koppie locality, only one of these sections was measured up to the apparent contact with the overlying Gemsbok River Formation and documents the approximate thickness of the entire Brak River Formation exposed at Koppie (Fig. 1C). The Brak River Formation is informally divided into lower, middle, and upper units, each separated by two 60 to 100 m thick mudstone-dominated intervals at the Koppie locality (Fig. 4C). The datum used for correlations made between the five Koppie sections is the base of the lower mudstone-dominated interval. Although correlations at the Koppie locality are the most robust in the study area because thick sandstone beds can be traced on aerial imagery and in the field, the desert varnish in this locality is more severe than at other localities, obscuring nearly all sedimentary structures and making it difficult to differentiate bed contacts between thin (<10 cm) beds in places. Thus, all five Koppie sections were measured at the decimetre-scale, due to poorer exposure of individual beds and internal sedimentary structures.

An additional stratigraphic section (Petroglyph) was measured in an adjacent fold limb, 1 km (*ca* 2 km restored) west of the northernmost Koppie section (Koppie 1; Fig. 1A). The Petroglyph section was measured at centimetre-scale and provides more detailed sedimentary features than any of the Koppie sections. At the Petroglyph section, only the lower to middle

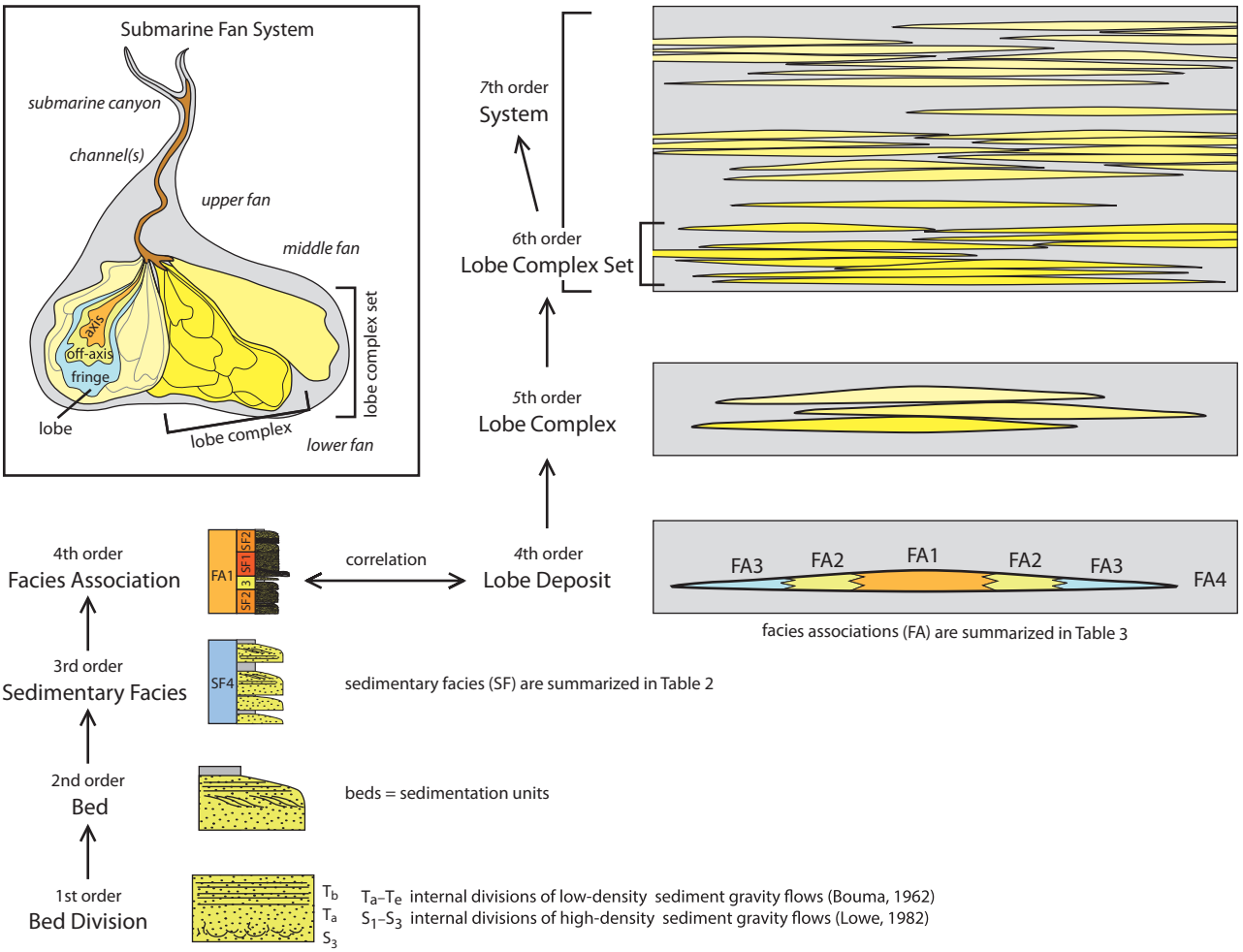

Fig. 3. Summary of architectural terms used to describe and interpret the deep-water lobe deposits of the Brak River Formation. Hierarchical scheme begins with (bottom left) first-order architectural elements that comprise internal divisions of low-density (T_a–T_e) and high-density (S_1–S_3) sediment gravity flow deposits that correspond to those assigned by Bouma (1962) and Lowe (1982), respectively. Second-order elements are composed of sedimentation units, or beds. Third-order elements are termed as sedimentary facies (SF1–SF6), and fourth order elements as facies associations (FA1–FA4), which are interpreted to represent lobe deposits. Refer to text and Tables 2 and 3 for more description. Lobe deposits, or lobes, stack to form lobe complexes, or fifth-order elements. Sixth-order elements are termed lobe complex sets. The seventh-order element represents the system and may represent a submarine fan. A schematic plan-form view of terms used in this hierarchical scheme is provided in the upper left.

Brak River Formation is exposed and the section can be correlated to the five Koppie sections by using the base of the lower mudstone-dominated interval as a datum. The Rhino Wash section (90 m section between Koppie and Temple localities; Fig. 1A: Appendix S2) is a partial stratigraphic section that cannot be correlated to the rest of the sections measured through the Brak River Formation, but exceptionally documents polished argillaceous sandstone and mudstone sedimentary facies (SF5 in Table 2), which is poorly exposed in other sections.

Temple

Only the upper Brak River Formation is exposed at the Temple locality and can be traced continuously for *ca* 5 km along the fold limb (Fig. 5). Three stratigraphic sections (named Waterfall, Staircase, and Tinter sections, from north to south) were measured and correlated. The datum used for correlations between the Temple sections is the base of a massive, blocky sandstone bed that lies directly above argillaceous sandstone and mudstone facies (SF5 in Table 2) and

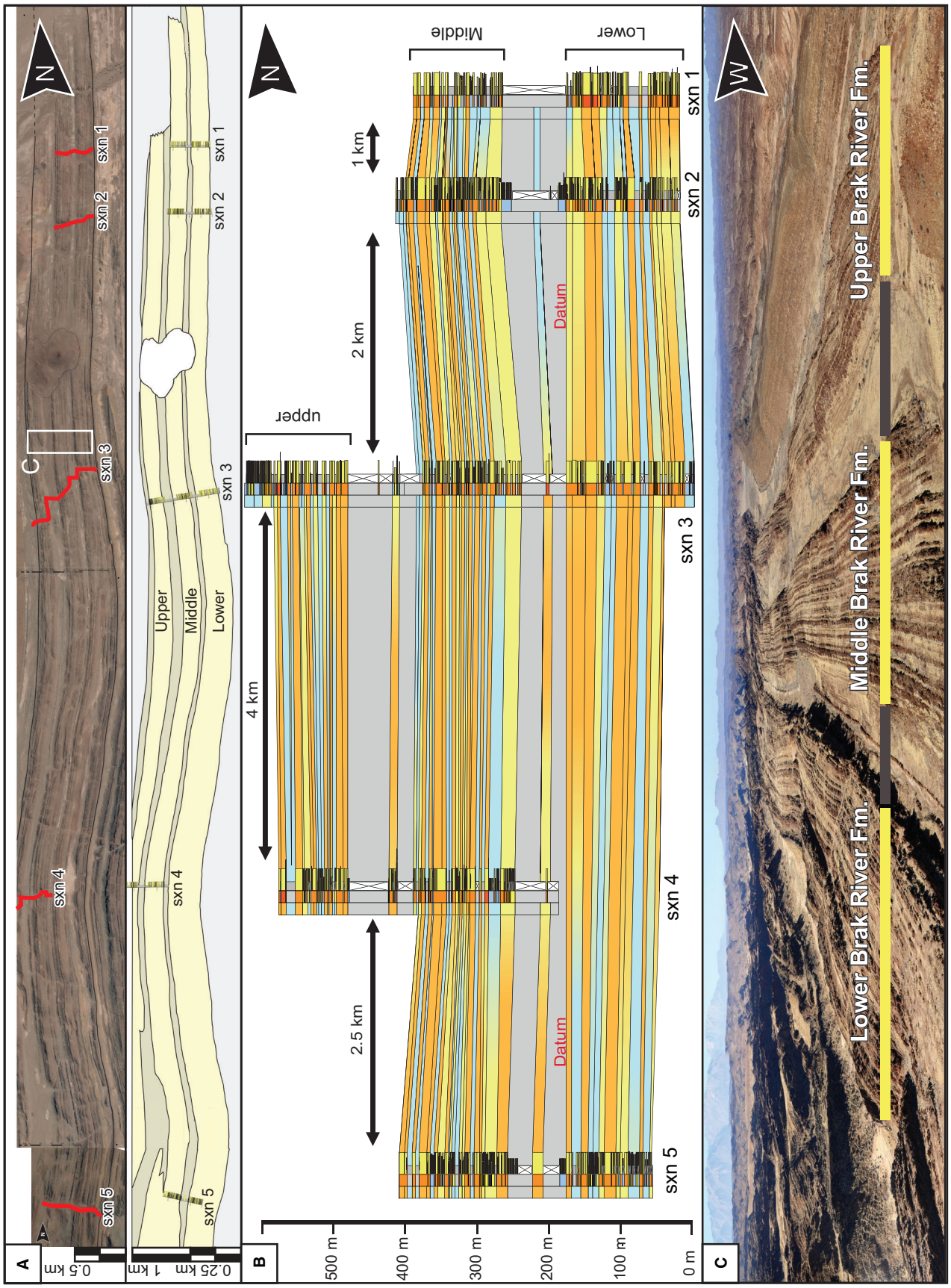

Fig. 4. (A) Satellite image (top) of Koppie locality, where five stratigraphic sections were measured. Red lines show transects of where each section (sxn) was measured in the fold limb. The interpreted panel below shows these sections draped over generalized stratigraphy (yellow = sandstone-rich; grey = mudstone-dominated intervals). (B) Five correlated Koppie sections. Gradient colours between correlation lines represent facies associations (FA) and their transitions between stratigraphic sections. Key for stratigraphic sections and correlations is the same as provided in Fig. 5. (C) Ground-view (looking south) of continuous stratigraphy (>10 km) with stratigraphic up to the right (west). Photographed area is labelled in satellite image in (A) and sandstone-rich versus mudstone-dominated intervals are once again highlighted with yellow and grey, respectively.

was laterally traced between each section, both with aerial imagery and mapping in the field. The top of the upper of two mudstone-dominated intervals was used as a datum to correlate the three Temple and five Koppie sections. The Tinter (farthest south) section at Temple is the only stratigraphic section that fully documents the top of the Brak River Formation and the transition into the overlying carbonate beds of the Gemsbok River Formation. All of the other sections that are measured up to the contact with the overlying Gemsbok River Formation are covered through this transition and thus the total thickness measurements are estimated.

Adderback

Adderback is the westernmost locality studied, lying roughly 30 km (*ca* 60 km restored) west of Koppie (Fig. 1A). Despite intense folding at Adderback, one complete representative stratigraphic section was measured at the centimetre-scale through the entire Brak River Formation (Fig. 6). This section is a composite of four partial sections that piece together better-preserved portions of the stratigraphy, avoiding minor faulting and the sheared upright limb of the complex fold (Fig. 6).

The Windy Wash section (33 m measured in Adderback; Appendix S2) documents exceptionally well-exposed thick-bedded, amalgamated sandstone facies (SF2 in Table 2). This detailed section lies somewhere in the upper Brak River Formation, although it could not be directly correlated due to local faulting and shearing.

PALAEOCURRENTS

Limited palaeocurrent data suggest an overall north to south/south-east direction of flow throughout the Brak River Formation (Fig. 7). The few measurements collected from sole marks (grooves and flute casts on the bases of beds) agree with those from ripple cross-laminations and with Swart (1992), who also interpreted an apparent flow direction largely from the north. Palaeocurrent data are limited due to the rarity of well-exposed ripple cross-laminations and are further complicated by the tight folding of the Zerrissene Group. In order to augment palaeoflow analysis, palaeocurrent measurements were also measured in part of the Amis River Formation (uppermost submarine fan deposits of the Zerrissene Group) where ripple cross-laminations are abundant and well-exposed, especially south-east of Adderback (Fig. 7). Although all palaeocurrent data from the Zerrissene Group may be somewhat compromised by rotation of the Ugab Region that may have accompanied the folding and shearing that has affected all rocks in the area, there is no evidence for any preferential rotation within the study area. There is some discrepancy in palaeocurrent data compared to previous work (e.g. Miller *et al.*, 1983a,b; Paciullo *et al.*, 2007), but broad scatter or obliquity of palaeoflow directions in deep-water systems are relatively common and can suggest deflections or dispersal of turbidity currents during deposition (Sinclair, 1994; Kneller & McCaffrey, 1999). Considering some degree of expected radiality, all data largely support a general southward palaeoflow direction (Miller *et al.*, 1983a,b; Swart, 1992; Paciullo *et al.*, 2007). Furthermore, sole mark measurements, which can be informative of flow type and activity (Peakall *et al.*, 2020) and are thought to better reflect principal flow direction measurements, more consistently support an overall north to south flow direction (Fig. 7). It can be expected for sole marks, which are interpreted to record basal and frontal flow directions, to be more consistent across a basin and show less variation than more dispersive current directions recorded by ripple cross-laminations, which can often be at high angles to the principal slope-controlled flow direction (Kneller *et al.*, 1991).

Table 2. Descriptions of sedimentary facies (SF) within the Brak River Formation.

Sedimentary facies (SF)	Bed thickness	Bed character	Bed characteristics and sedimentary structures	Depositional processes
SF1: Thick-bedded, scouring sandstone with basal mudstone–clast conglomerate; sparse graels and cobbles	50–100 cm; 2–70 cm scours	Scouring, irregular, and lenticular; rare flat amalgamation surfaces	Clast-supported mudstone–clast conglomerate; clast-supported may grade to matrix-supported, then grades to massive sandstone; dropstones relatively common	Erosive high-density turbidity current
SF2: Thick-bedded, amalgamated sandstone; no mudstone–clast conglomerate	50–100 cm; thicker where amalgamated	Tabular to irregular; scoured where irregular; commonly amalagamated	Abundant massive (T_a/S3) division, planar lamination (T_b), minor ripple lamination (T_c), dish structures, flame structures, flute casts/grooves on flat bases, dropstones throughout	Collapsing high-density turbidity current or sustained, steady flow; debris flow in rare cases
SF3: Medium-bedded sandstone and mudstone	20–50 cm	Predominantly tabular; rarely amalgamated	Massive (T_a/S3) division, planar to wavy lamination (T_b), ripple lamination (T_c), loaded mudstone caps (T_e)	Sustained, low-density turbidity current
SF4: Thin-bedded sandstone and mudstone	1–20 cm	Tabular	Thin massive (T_a), planar (T_b), ripple lamination (T_c), mudstone caps (T_e)	Waning low-density turbidity current
SF5: Argillaceous sandstone and mudstone	1–50 cm	Tabular	Mud-rich sandstone with mud content increasing up; rare ripple lamination at top of beds; mudstone clasts; some banding; dropstones throughout	Transitional flow with both turbulent and cohesive properties
SF6: Massive mudstone and siltstone	50–800 cm	Little to no bedding; tabular where preserved	Sheared and metamorphically altered (highly cleaved)	Off-axis/distal hemipelagic settling with rare, low-density turbidity current

HIERARCHICAL SCHEME

The development of hierarchical schemes for architectural elements is meant to facilitate the documentation and characterization of various scales of observation for a particular system. Thus, the scheme is tailored to the particular outcrop of study and also placed in a general, conventional framework established for deep-water settings so that different hierarchies are somewhat comparable between different systems. To enable the comparison of the Zerrissene system to other well-defined hierarchies specific to deep-water lobe deposits, this study presents the hierarchy defined for the Brak River Formation of the Zerrissene Group in the context of the Permian Tanqua Karoo (Prélat *et al.*, 2009), Eocene–Oligocene Annot Sandstone system (Mulder & Etienne, 2010), and Neoproterozoic Windermere Supergroup (Terlaky *et al.*, 2016) in Table 1.

In order to best characterize the Brak River Formation and its spatial distribution, a hierarchical scheme of architectural elements is adopted (Fig. 3). The finest scale discussed, representing first-order architectural elements of Ghosh & Lowe (1993), comprises internal divisions of low-density (T_a–T_e) and high-density (S_1–S_3) sediment gravity flow deposits that correspond to those assigned by Bouma (1962) and Lowe (1982), respectively. Second-order elements are composed of sedimentation units, or beds. Third-order elements are termed as sedimentary facies (SF1–SF6), and defined as mappable groupings of similar beds, based on observations of bed thickness, grain size, and sedimentary structures (equivalent to lithofacies of Ghosh & Lowe, 1993). Sedimentary facies of the Brak River Formation, summarized in Table 2, can be internally variable (for example, there is rare mudstone separating the sandstone beds of thick amalgamated sandstone facies, SF2, where flows were not always erosive enough to eliminate thin mudstone caps). Facies associations (FA1–FA4), or fourth-order elements, are summarized in Table 3, and were assigned based on groups of genetically related sedimentary facies that represent distinct depositional processes.

Facies associations are interpreted to represent lobe deposits. These stack to form lobe complexes, or fifth-order elements (Fig. 3). Sixth-order elements are termed lobe complex sets (Fig. 3). A seventh-order architectural element is defined as a system and is discussed as the submarine fan system (Fig. 3). The submarine fan system, or largest scale architectural element used to describe the Brak River Formation and/or Zerrissene Group, includes both semi-confined and unconfined elements. The terminology used describes the submarine fan system as an overarching system that extends from submarine canyon to the most distal reaches of the largely unconfined, depositional apron and includes small distributive channels and depositional lobes as smaller-scale architectural elements that are commonly associated with the lower fan environment (Bouma *et al.*, 1995).

SEDIMENTARY FACIES

Six distinct sedimentary facies were recognized in the Brak River Formation (Table 2; Fig. 8): (i) thick-bedded (50 to 100 cm thick), erosive sandstone with basal mudstone-clast conglomerate (SF1); (ii) thick-bedded (can be thicker than 100 cm, if amalgamated) sandstone without mudstone-clast conglomerate (SF2); (iii) medium-bedded (20 to 50 cm thick) sandstone and mudstone (SF3); (iv) thin-bedded (1 to 20 cm thick) sandstone and mudstone (SF4); (v) argillaceous sandstone and mudstone (SF5); and (vi) massive mudstone and siltstone (SF6). Beds are interpreted as individual sedimentation units resulting from sediment gravity flows, including turbidity currents, debris flows, and transitional (hybrid) flows. Few outliers in bed thickness exist within these divisions. Outcrop expressions of sedimentary facies are shown in Fig. 8.

SF1: Thick-bedded sandstone with basal mudstone-clast conglomerate

Description

Thick-bedded sandstone with basal mudstone-clast conglomerate represents the coarsest facies observed in the Brak River Formation. Sandstone beds are 50 to 100 cm thick, and underlying mudstone-clast conglomerate fills lenticular geometries ranging from 0.1 to 2.5 m deep, but more commonly 0.25 to 0.7 m deep and up to 30 m wide. Mudstone clasts that are the defining characteristic of SF1 are sub-angular to rounded (commonly elongated), range from <1 to 10 cm in diameter, and are clast-supported, and hence are referred to as a conglomerate (Fig. 8C and D). Clast-supported basal conglomerates often grade into matrix-supported, then to massive sandstone higher in the bed.

Sub-angular to angular, granitic granules–pebbles and exotic (i.e. quartzite, granite, and basalt),

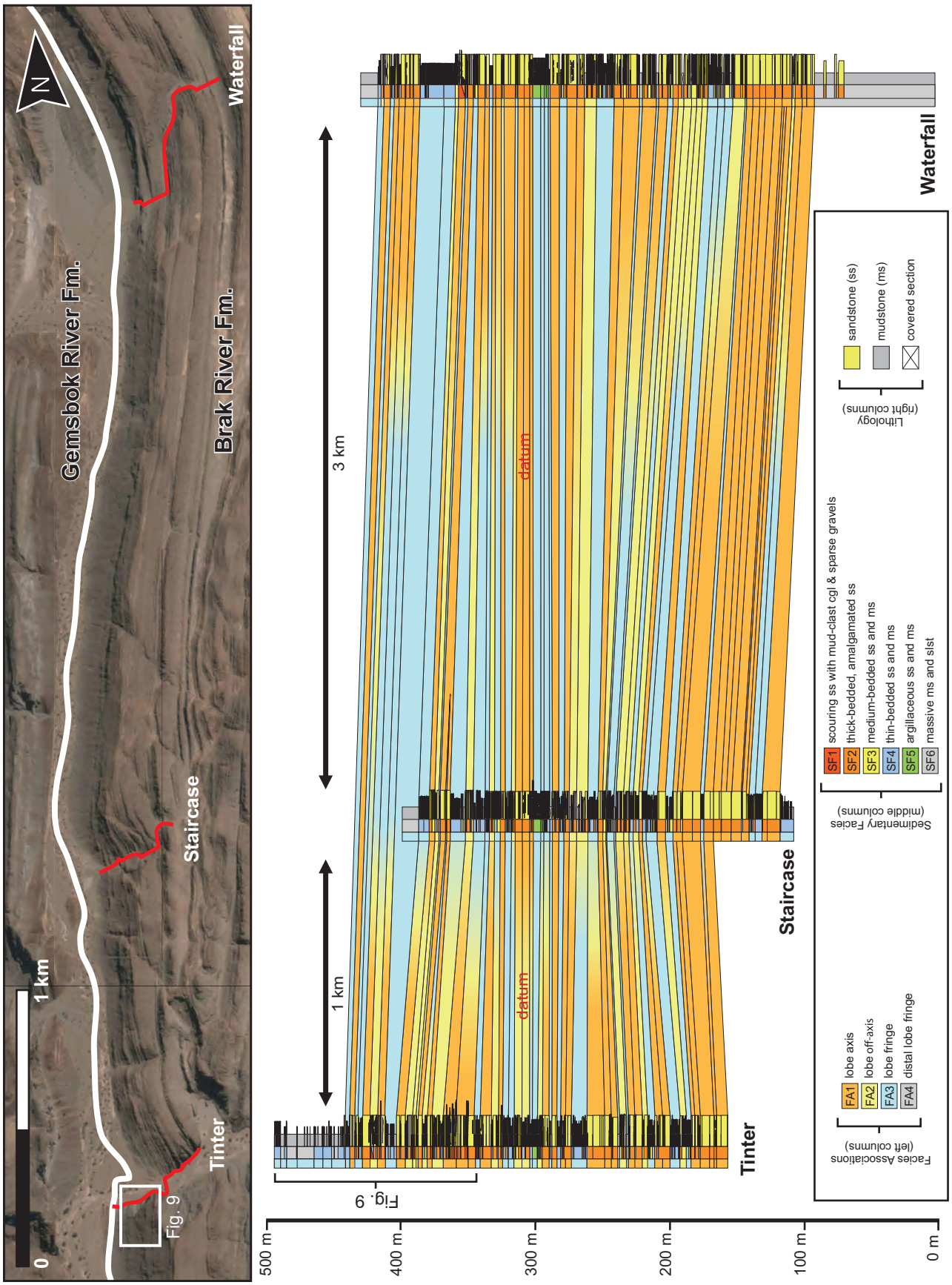

Fig. 5. Satellite image (top) of Temple locality highlighting the three stratigraphic sections measured. Red lines trace the path taken along the exposure to measure each section in the field. White line traces the contact between the Brak River Formation and the overlying Gemsbok River Formation. Gradient colours between correlation lines made between three Temple sections represent facies associations (FA) and their transitions between stratigraphic sections.

sub to well-rounded cobbles are intermixed with some of the mudstone-clast conglomerate. In only one instance, granitic granules–pebbles are observed at a relatively flat amalgamation surface and unrelated to mudstone-clast conglomerate (Fig. 8B). Exotic cobbles are often observed higher in sandstone beds, unrelated to basal mudstone-clast conglomerates.

Interpretation

The presence of mudstone-clast conglomerate at the base of scours indicates deposition from energetic, erosive flows that are most likely representative of a more proximal or axial lobe setting. Mudstone clasts were intrabasinal, or locally derived from energetic flows that removed the T_d and T_e divisions of immediately underlying beds. Mudstone clasts more rarely observed near the tops of sandstone beds in SF1 reflect clasts that, instead of being disaggregated or deposited at the base of erosive flows, were worked into the flow, and settled higher/later in the flow at hydraulic equivalence. Cobbles found throughout sandstone beds and unrelated to erosive basal scours, are interpreted to be glaciogenic dropstones that fell into the system from melting ice cover above and deposited in random positions in sandstone beds during their accumulation (Miller *et al.*, 1983a; Swart, 1992, 1994). This interpretation is supported by the diverse compositions of the cobbles, reflecting lithologically varied sources that were tapped by glaciers, transported, and ultimately dropped into the Zerrissene system. Disruption of bedding, such as loading of bed laminae (Fig. 9H), is commonly observed in association with dropstones, providing further evidence for glaciogenic origin. One unique exposure preserves a dropstone ahead of a drag mark on the base of a bed (Fig. 9G) that likely records a dropstone that was entrained and dragged by a turbulent flow along a discontinuous, irregular path near the base of the bed. These dropstones are unrelated to flow type in the Brak River Formation, but reflect glacial activity documented globally at this time (e.g. Hoffman *et al.*, 1998), likely recording the global-scale Marinoan Glaciation (Nieminski *et al.*, 2019).

Cobbles that are found within mudstone-clast conglomerate in basal scours are interpreted to be glacial dropstones that were picked up, entrained, and re-deposited by more energetic, erosive flows that were capable of carrying the coarsest material present in the system. These cobbles are commonly intermixed with sparse granules–pebbles (Fig. 9D) but have characteristic differences, including: (i) granules are less variable in clast size than the cobbles; (ii) granules–pebbles are relatively uniform in composition; all are sub-angular-to-angular, dark, and of plutonic composition, suggesting a granitic source, whereas cobbles, or dropstones, are of diverse and exotic origin; and (iii) granules–pebbles appear exclusively in erosive bases of beds, never throughout sandstone beds, providing no evidence for characteristic dropstone behaviour for this clast-size fraction. Thus, it is possible that rare granules–pebbles represent a source that is distinct from that of the dropstones commonly found in the same erosive bases. Otherwise, these granules–pebbles may represent reworked glacial detritus.

SF2: Thick-bedded sandstone without basal mudstone-clast conglomerate

Description

SF2 is characterized by dominantly stacked, commonly amalgamated, sandstone beds that range from 50 to >100 cm thick (Fig. 8A). Irregular bed bases can occur in SF2, but no mudstone-clast conglomerate is observed. Thick sandstone beds of SF2 are predominantly structureless. Some show planar and ripple cross-laminations. These are often capped by a planar laminated siltstone upper interval. At Windy Wash (Adderback locality) SF2 beds range from 0.25 to 10.7 m thick, but are most commonly 1 to 4 m thick, exhibit no grading, and yet are rarely entirely massive. These beds often display dish structures from dewatering during sedimentation, diffuse planar to wavy laminations, ripple cross-laminations near the bases and tops of beds, and commonly structured siltstone intervals below mudstone caps (Fig. 9B). Mudstone caps never exceed 10 cm in thickness and are not abundant. Sandstone beds more commonly grade normally into planar-laminated siltstone.

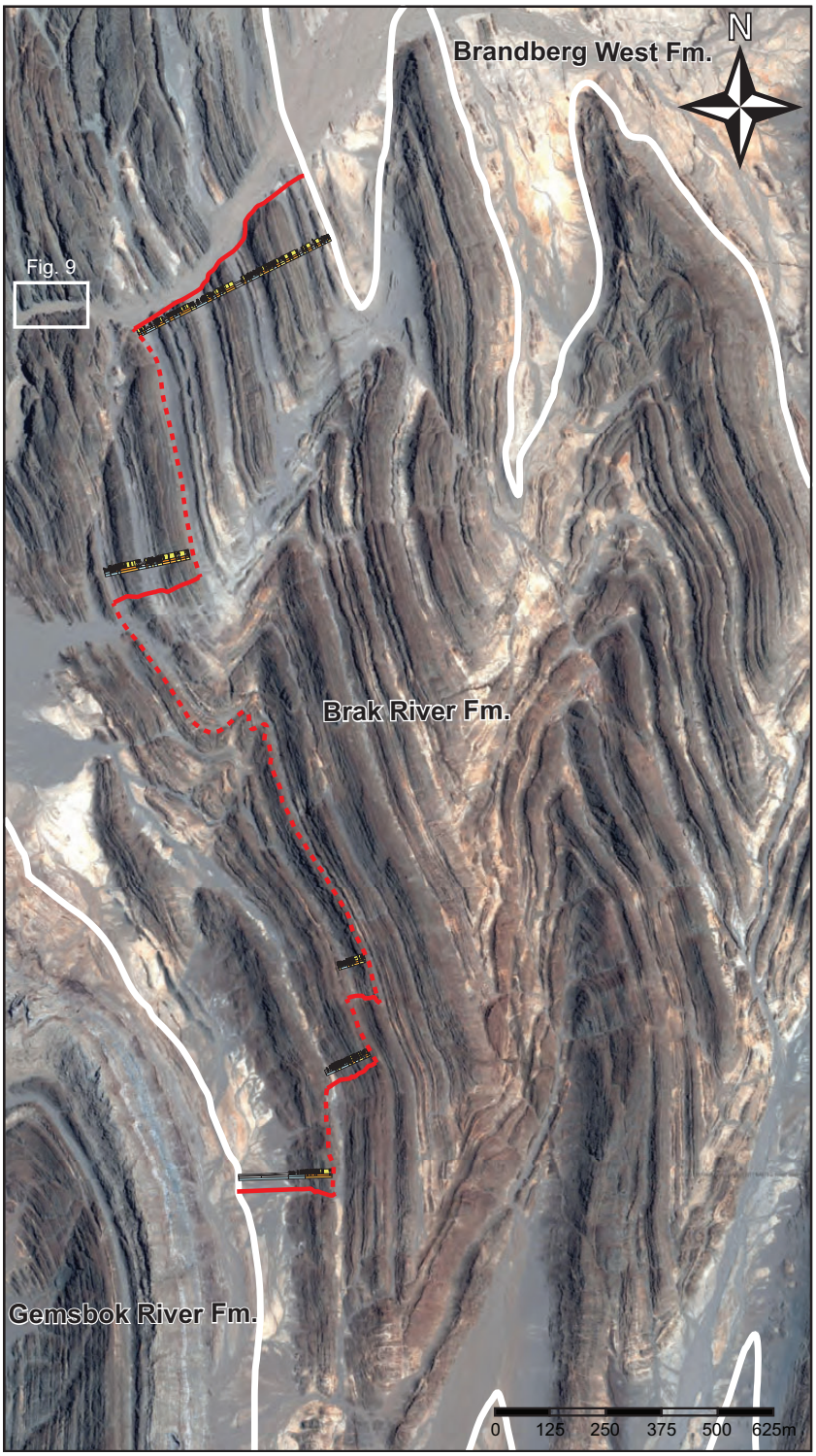

Fig. 6. Satellite image of Adderback locality where the Adderback composite stratigraphic section was measured through the entirety of the Brak River Formation. Stratigraphic up is to the west. Solid red lines trace where each partial section was measured in order to measure stratigraphy where best exposed; dashed red lines mark how each partial section was pieced together as beds were traced between tight fold limbs. Five partial sections are overlain over the satellite image to the side of each solid red line. Refer to Fig. 13 for full measured stratigraphic section of partial sections stacked on top of one another. Location of Windy Wash section (Fig. 9; Appendix S2) is indicated.

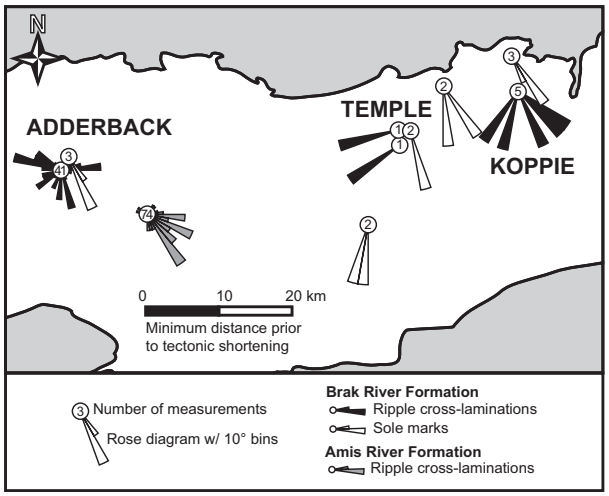

Fig. 7. Rose diagrams of palaeocurrent data shown spatially across the Zerrissene basin prior to ≳50% east–west tectonic shortening. Grey shaded areas outline the exposure of the Zerrissene Group (in white). Data is shown for measurements of ripple cross-laminations and sole marks from the Brak River Formation and are supplemented with additional measurements from the overlying Amis River Formation collected in one location.

Amalgamation surfaces are frequently flat and subtle. They usually are not marked by a distinct grain size or other lithological changes but can be identified with thin (1 to 2 cm thick) mudstone clast horizons (Fig. 9A). Flame structures are also common at bed contacts from loading by the overlying bed (Fig. 9E). Finer-grained units that are preserved between sandstone portions of beds can also show flame structures or other effects of sediment loading (Fig. 9F). Additional features observed in SF2 include flute casts and grooves (occurring separately) that are common on the undersides of thick sandstone beds, and rarely associated with other sedimentary facies (Fig. 9G).

The thickest bed documented in the Windy Wash section is 10.7 m in thickness and has a 3.6 m thick massive base, above which are *ca* 60 cm thick alternating intervals of faint planar to wavy laminations and massive sand. The uppermost 30 cm of this bed grades normally to planar-laminated siltstone and is capped by 10 cm of mudstone. Glacial dropstones occur throughout, in both massive and structured intervals of the bed, and are most commonly well-rounded and found as the nucleus for concretions (Fig. 9C). Many sandstone beds in the Windy Wash section have isolated dropstones in the middle or near the top of beds, occasionally loading or vertically deforming bedding (Fig. 9G

Table 3. Descriptions of facies associations (FA) within the Brak River Formation.

Facies association (FA)	Sedimentary facies (SF) (Table 1)	Sedimentary characteristics	Depositional environment
FA1	SF1 and SF2 dominant; also intermixed SF3 and subordinate SF4	Sandstone-dominated, but with common thin-bedded sedimentary facies between sand-rich packages; >90% sandstone	Lobe axis: records the majority of sand deposition in the system; erosive; otherwise flows lose confinement and collapse rapidly; more proximal and/or axial
FA2	SF2, SF3; less frequent SF4 and SF5; minor SF6	Relatively sand-rich but with intermittent mudstone; predominantly medium- to thick-bedded sandstone sedimentary facies; *ca* 70% sandstone	Lobe off-axis: realm of relatively sand-rich, and exclusively unconfined flows that are lower in energy and/or higher in mud contnet (i.e. transitional flows) than more proximal/axial in the lobe system
FA3	SF4, SF5, SF6; minor occurrence of SF3; relatively rare SF2	Consisting of lower-energy sedimentary facies, but with wide distributions of bed thickness and sandstone abundance; *ca* 50% sandstone	Lobe fringe: distal from the highest energy flows or any main sediment fairway; lower in energy
FA4	SF6; relatively thick and uninterrupted	Thick, mudstone-dominated intervals that are through-going and semi-regional; rarely interrupted by thin sandstone beds; <20% sandstone	Distal lobe fringe: away from active lobe deposition; does not record a system shut-off, but rather a relative shift of sand deposition to elsewhere in the basin

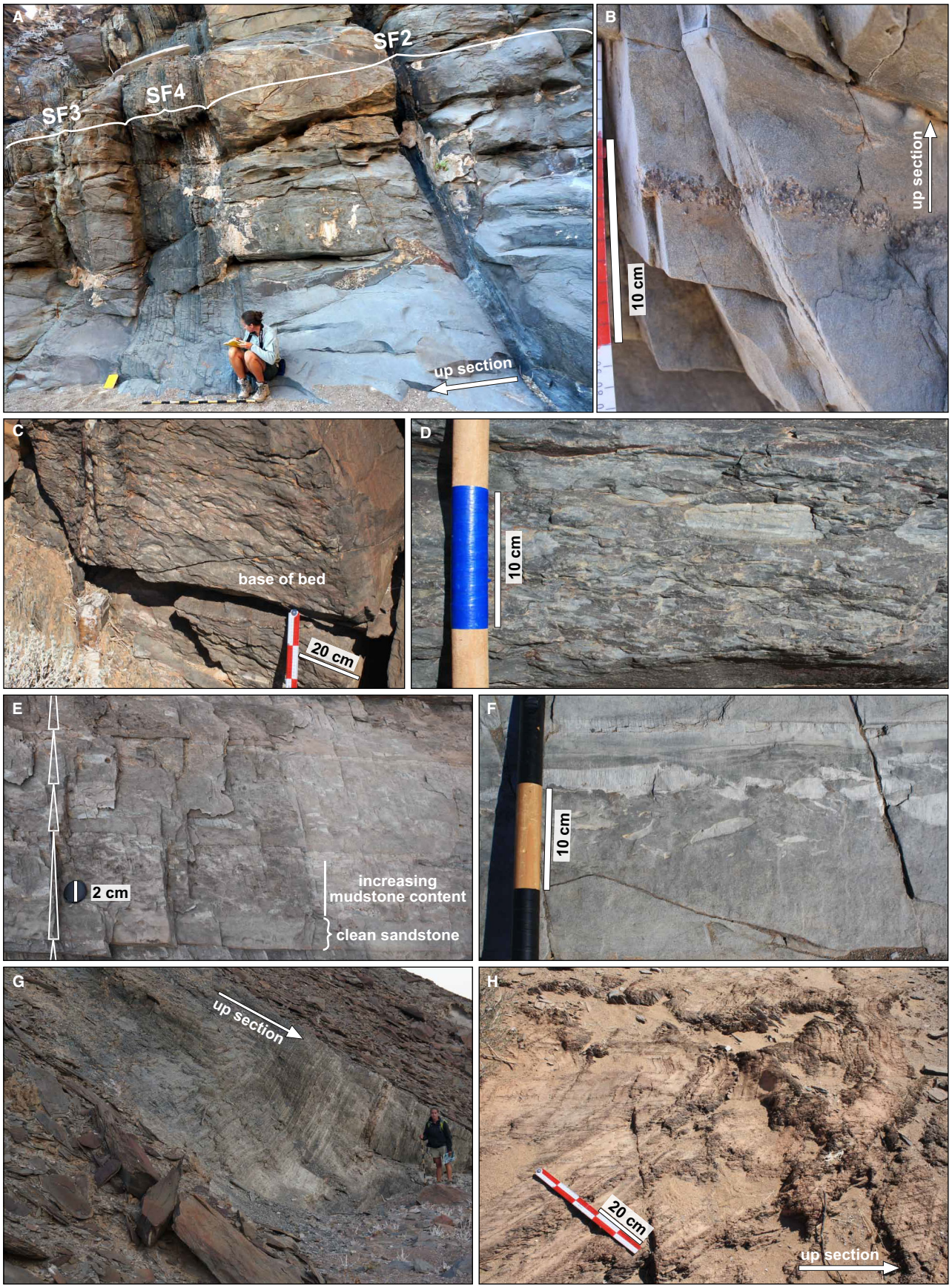

Fig. 8. Examples of each of the six sedimentary facies (SF) and their outcrop character. (A) General distinction and bedding differences between SF2 (thick-bedded, amalgamated sandstone), SF3 (medium-bedded sandstone and mudstone), and SF4 (thin-bedded sandstone and mudstone). (B) Rare granules found at the base of thick-bedded, scouring sandstone (SF1) beds. (C) Base of SF1 bed highlighting roughly 10 cm of mudstone-clast conglomerate that dominates erosive bases of SF1. (D) Close-up of poorly sorted, stretched mudstone clasts in SF1. (E) Argillaceous sandstone and mudstone (SF5) beds, each with 1 to 2 cm of cleaner (mud-poor) sandstone at the base, below an abrupt transition to an increasing concentration of mudstone clasts above. Note that sandstone is darker grey and mudstone clasts are lighter in colour. (F) Close-up of a single SF5 bed with a clean sandstone base, upward-increasing mudstone clasts appearing in the middle of the bed, and faint current structures just below a mudstone cap. (G) Thin-bedded sandstone and mudstone (SF4). Person for scale is *ca* 1.8 m tall. (H) Highly deformed and rarely exposed massive mudstone and siltstone (SF6).

and H). Isolated mudstone clasts are also common near the tops of thick sandstone beds.

Interpretation

The origin of massive sandstone beds in deep-water systems and the rheology of their depositing flows has been a topic of debate for several decades (e.g. Lowe, 1982; Kneller & Branney, 1995; Shanmugam, 1996; Baas, 2004). Although these beds are generally deposited from suspension of collapsing flows, they can be complex and relatively variable, representing a few different types of environments (Stow & Johansson, 2000) and invoking slightly different depositional processes (Lowe, 1982; Kneller & Branney, 1995). The relatively high abundance of entirely massive sandstone beds that is recorded in the Brak River Formation, and perhaps in analogous turbidite systems as well, is questionably overrepresented due to quality of exposure. For this reason, the 30 m thick Windy Wash section was measured to better document well-exposed, seemingly massive, thick sandstone beds.

Massive sandstone beds in the Brak River Formation are consistent with the S_3 division of high-density turbidity current deposits (Lowe, 1982) and the T_a division of low-density turbidity currents (Bouma, 1962). Massive SF2 beds in the Brak River Formation are interpreted to have been deposited by sustained, steady flow or, in some cases, by rapid deposition by collapsing high-density turbidity currents, as evidenced by dewatering structures. Thicker massive beds did not result directly from thicker flows, but rather are interpreted to reflect longer-lived quasi-steady flows (Kneller & Branney, 1995). Vertical variations in the beds, such as changes from massive character to planar laminations (T_b) and ripple cross-laminations (T_c) above that, do not suggest direct variation in the vertical structure of the depositing flows, but rather reflect temporal changes in the depositing currents (Kneller & Branney, 1995). Thin siltstone to mudstone caps (T_d/T_e), where present, represent the slow deposition of fine material from the tails of low-density turbidity currents. Amalgamation of deposits reflects erosion of any fine-grained material, but the generally tabular geometries of SF2 suggest that the flows were not strongly erosive like those that deposited beds of SF1. Isolated mudstone rip-up clasts imply that flows were more erosive upstream, where they were energetic enough to rip up partially consolidated mud from the seafloor and/or previous deposits. These clasts of relatively unconsolidated mud were then incorporated into the upper portions of the high-density flows.

SF3: Medium-bedded sandstone and mudstone

Description

SF3 is dominated by beds that range from 20 to 50 cm thick. The sandstone beds are tabular, rarely amalgamated and are separated by mudstone (Fig. 8A). Beds are normally graded, most commonly with a massive sandstone interval at the base, overlain by planar laminated sandstone and an uppermost mudstone interval. Ripple laminations are also common below the mudstone interval. Although water escape structures, such as dish and pillar structures, are not found in SF3, some wavy laminations and centimetre-scale loading features (Fig. 9F) are present. Mudstone clasts from 1 to >10 cm in length, where present, are always found towards the tops of sandstone beds, but are not nearly as common as in SF2 and are not found at the base of beds or as mudstone-clast conglomerates, as in SF1.

Interpretation

SF3 beds were deposited by low-density turbidity currents. The flows were likely sustained

Fig. 9. Select examples of sedimentary features best observed in the detailed Windy Wash partial stratigraphic section (provided in Appendix S2) measured to characterize thick-bedded, amalgamated sandstone facies (SF2). Refer to Figs 1A and 6 for section location. Orange knife pictured is 10 cm in length. Where marked, 'up section' indicates the depositional 'up' direction, perpendicular to bedding, which can easily be mistaken with metamorphic cleavage in these outcrops. (A) Amalgamation surface of thick-bedded sandstone beds marked by a mudstone-clast horizon. (B) Dish structures partway up a thick-bedded sandstone bed with a massive (structureless) base (not pictured). (C) Later-stage concretion that formed around a glacial dropstone (in its centre), in the middle of thick-bedded sandstone. (D) Gravel bed at the base of an erosive thick-bedded sandstone bed (SF1) with two glacial dropstones that have been reworked by the coarser-grained, erosive flow. (E) Large-scale flame structure from loading commonly observed in SF2 and SF3 (smaller scale). (F) Sediment loading of SF3 by thick sandstone bed of SF2 (dark-coloured base of SF2 bed at the very top of image). (G) Drag mark left by a dropstone. (H) Large dropstone and resulting deformation of laminae.

and unconfined. Some low-density turbidity currents were energetic and erosive enough to pick up mud from previously deposited sediments and incorporate it as mudstone rip-up clasts in overlying turbidites. None appear to have been as energetic as the more deeply erosive and scouring flows that deposited SF2. Load features and soft sediment deformation record foundering and sinking of denser sands into the water-saturated, soft muds and silts deposited by preceding flows.

SF4: Thin-bedded sandstone and mudstone

Description

SF4 is dominated by tabular sandstone beds (1 to 20 cm thick; Fig. 8G) with well-defined mudstone caps. Average percent sandstone is roughly 50% and bed thickness is uniform, with no lenticularity at the outcrop scale. Bed contacts are typically flat. SF4 sandstone is finer grained than SF1 and SF2. Some successions are primarily composed of mudstone with 2 to 10 cm thick sandstone stratigraphically spaced 10 to 40 cm apart. Commonly, the sandstone beds show a vertical trend of decreasing thickness that transitions into SF6. Otherwise, SF4 is commonly abruptly present between much more sandstone-rich SF2 and SF3 intervals (Fig. 8A).

Interpretation

SF4 preserves well-developed partial to nearly complete (T_a–T_e) Bouma sequences (Bouma, 1962) and records deposition by lower-energy, waning, low-density turbidity currents. Tabular bedding geometries suggest that the flows depositing these beds were non-erosive, unconfined, and likely deposited in the most off-axis/distal regions, after the majority of sand was deposited up dip or more axially.

SF5: Argillaceous sandstone and mudstone

Description

Argillaceous sandstone and mudstone beds of SF5 demonstrate an overall greater mudstone content throughout the sandstone portion of the bed. This increase in mud content is often reflected by an upward increase in abundance of matrix-supported mudstone clasts (Figs 8D and 10A), but can otherwise be visually identified by a greater degree of reflected light, or sheen (that characterizes metamorphosed siltstone and mudstone), in the more mud-rich sandstone of SF5 (Fig. 10B), compared to cleaner (mud-poor) sandstone beds. The change in mud concentration relative to sheen in outcrop is confirmed by thin sections (Fig. 10C and D) and results from metamorphosed chlorite and likely sericite, which gives phyllite (low-grade metamorphosed mudstone) its sheen (e.g. Goldstein Jr & Reno, 1952). SF5 bed thickness ranges from 5 to 95 cm, of which the thinner beds (<15 cm) occur together as discrete packages. Sedimentary structures such as planar or current ripple laminations, or water escape structures are rare within argillaceous sandstone facies; however, characteristic banding can be observed (Fig. 10J). Banding divisions (cleaner, mud-poor versus more mud-rich) vary in thickness (0.1 to 10 cm) and are sub-parallel to parallel (thickness does not change laterally). Contacts between bands are commonly sharp and flat, although depending on outcrop exposure some contacts appear more diffuse, particularly between thinner bands. Internal details of banding such as loading of one banding division by the other or interbedded planar lamination, if present, are challenging to observe, making it difficult to assess whether banding in this system likely records episodic near-bed damping of turbulence (Lowe & Guy, 2000) or tractional

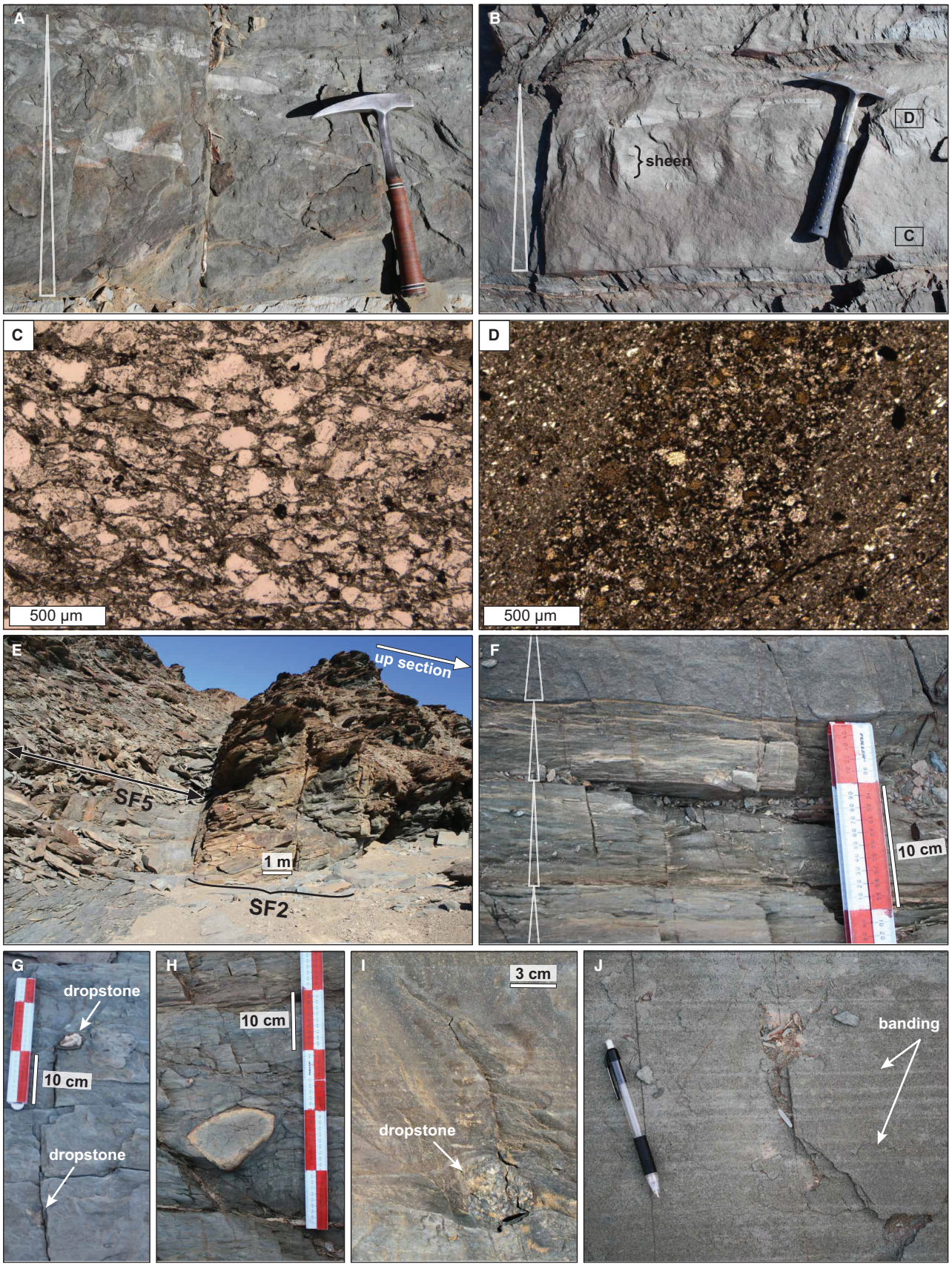

Fig. 10. Select features observed in argillaceous sandstone and mudstone (SF5) beds, which were best characterized in the Rhino Wash partial section (Appendix S2) measured to fully document this facies. Refer to Fig. 1A for section location. (A) SF5 bed with increase in mudstone content reflected by an increase in mudstone clasts through the bed. Rock hammer is 33 cm in length. (B) SF5 bed that exhibits a great 'sheen', or higher reflectance of light, indicating an increase in mudstone content through the bed. Thin sections were cut from two samples collected from the approximate locations indicated in right of the image. Rock hammer is 23 cm in length. (C) Photomicrograph (in planar light) of a thin section sample collected from the base of the SF5 bed shown in (B). (D) Photomicrograph (in planar light) of a thin section sample collected from near the more mudstone-rich top of the SF5 bed shown in (B). (E) Outcrop photograph taken of SF5 package measured in Waterfall section, at Temple, highlighting the common vertical relationship of SF5 abruptly overlain by SF2, sometimes partially scoured by SF1 (for example, at this horizon correlated *ca* 3 km to the south, at Staircase section). (F) Variable degree of mudstone content in SF5. Bottom three beds are mudstone-rich throughout; uppermost bed is the relatively sand-rich base of an SF5 bed beyond the photograph. (G, H) Dropstones preferentially found in many SF5 beds. (I) Dropstone disrupting laminae. (J) Banding observed in argillaceous sandstone bed. Pencil is *ca* 14 cm in length.

bedform reworking and development (Baas *et al.*, 2011; Stevenson *et al.*, 2020).

SF5 beds are only observed in the Temple and Koppie (only Sections 2 and 5) localities (Appendix S1). SF5 beds are laterally continuous in the Temple locality, where a distinct package of SF5 beds in the upper Brak River Formation is correlated over nearly 5 km between the three stratigraphic sections, thinning from 11 m thick in the Waterfall section to 4 m thick in the Tinter Section, 4 km south (Fig. 5). The maximum thickness of individual SF5 sandstone beds thins southward in each of these measured sections as well (from 95 cm at Waterfall to 15 cm at Tinter; Appendix S1). These trends document thinning in the overall down-flow direction (Figs 5 and 7). The correlated package records a common occurrence of dropstones (Fig. 10G to I), which are otherwise only commonly associated with SF1 and SF2 beds. In thinner SF5 beds, some large dropstones, which reach 5 to 30 cm diameter, lie along bed contacts.

In every correlated section in which SF5 is observed, there is a lateral correlation and/or vertical relationship between the argillaceous facies and mudstone-clast conglomerate beds (SF1) and/or thick-bedded amalgamated sandstone beds (SF2; Fig. 10E). An erosive and lenticular package of SF1 beds directly overlies the package of SF5 correlated between two of the three sections at Temple, in the Tinter and Staircase Section (Fig. 5; Appendix S1). A 3 m thick package of SF5 identified in Section 2 at Koppie is correlated to a 6 m thick SF1 package with 30 cm of mudstone-clast conglomerate at its base in Section 1, just 1 km to the north (Fig. 4). Similarly, a 1.6 m thick SF5 package in Section 5 at Koppie is correlated to 2.5 m of SF1 with 80 cm of mudstone-clast conglomerate at its base in Section 4, *ca* 2.5 km to the north (Fig. 4).

Interpretation

Transitional flows are more mud-rich and suggest involvement of both turbulent and laminar, or cohesive, flow (Lowe & Guy, 2000; Lowe *et al.*, 2003; Haughton *et al.*, 2009; Baas *et al.*, 2011). Although controversy still exists as to the rheological behaviour of transitional flows, field observations and laboratory efforts continue to better constrain their origin and variability (e.g. Talling, 2013; Baker *et al.*, 2017). The presence of argillaceous sandstone beds, also termed slurry beds (*sensu* Lowe & Guy, 2000), hybrid event beds or linked debrites (*sensu* Haughton *et al.*, 2009), and transitional flow deposits (*sensu* Kane & Pontén, 2012, and used here), are commonly found: (i) in distal parts of an unconfined depositional system (*cf.* Hodgson, 2009; Talling *et al.*, 2012; Talling, 2013; Kane *et al.*, 2017); or (ii) as avulsion splay deposits (*cf.* Terlaky & Arnott, 2014). Although argillaceous sandstone facies (SF5) are not abundantly observed in the Brak River Formation, possibly due to the difficulty in identifying these beds in exposures that are not polished, observations were made that offer insight into the depositional context of transitional flows in the Zerrissene system.

Argillaceous sandstone beds (SF5) in the Brak River Formation are interbedded with turbidites and, in some cases, correlate laterally with low-density turbidite deposits (for example, Koppie; Fig. 4). In every case where SF5 beds are observed, they either coincide vertically or correlate down palaeo-transport direction (Fig. 7) from mudstone-clast conglomerate facies (SF1), suggesting that deposition of SF5 beds is dependent on the presence of SF1 beds up-dip. The authors interpret that argillaceous sandstone beds are a down-flow or semi-lateral result of

erosive, sand-rich, turbulent flow that entrains mud-rich sediment by eroding into underlying muddy seafloor substrate and disaggregating mud-clasts during transport, becoming a transitional flow that deposits argillaceous sandstone down palaeo-transport direction of erosive mudstone-clast conglomerates (*cf.* Power *et al.*, 2013; Terlaky & Arnott, 2014). Transitional flow deposits in the Brak River Formation also preserve a relatively high concentration of dropstones compared to other sedimentary facies. The occurrence of dropstones is otherwise only observed in SF1 and SF2, which are closely related to the few transitional flow deposits recorded, as discussed above. The relationship between dropstones and argillaceous sandstone and mudstone beds has not previously been documented in other systems. It may suggest a relationship between ice cover and an increased glaciomarine input of silt and clay to the deep-water system which, in turn, would have been incorporated sufficiently into overriding turbidity currents to develop into transitional flows.

SF6: Massive mudstone and siltstone

Description

SF6 encompasses mudstone and siltstone with little to no sandstone. Sandstone beds are almost entirely absent. SF6 mudstone intervals do not include mud caps that represent the uppermost parts of sand-rich sedimentation units, but rather thicker intervals of mudstone that show no evidence for being associated with any sandstone beds. Within this facies, 1 to 5 cm thick quartz veins are abundant and the depositional fabric is often highly deformed (Fig. 8H). It is clear that the mudstone facies of SF6 experienced most of the tectonic strain of the Zerrissene Group, as evidenced by the abundant secondary quartz veins and intense deformation. These mudstone-dominated intervals are most commonly covered throughout the field area, and thus are often inferred, except along eroded and polished stream wash walls.

Interpretation

SF6 represents very low-energy deposition in an interval in which sandstone deposition was locally absent for an extended period of time, apart from a few anomalous, very thin sandstone beds. This facies was deposited at spatial positions where there was infrequent low-density turbidity current input (e.g. Boulesteix *et al.*, 2020).

FACIES ASSOCIATIONS

The Brak River Formation is characterized by four facies associations (FA1–FA4; Table 3) that are distinguished as groups of genetically related sedimentary facies (SF1–SF6; Table 2) and are described below. Representative stratigraphic sections of each facies association, with dominant sedimentary facies highlighted within, are depicted in Fig. 11. Outcrop expressions of facies associations are shown in Fig. 12. Collectively, the facies associations are interpreted to represent deposition within a deep-water lobe environment in a lower submarine fan setting (see Reading & Richards, 1994; Bouma *et al.*, 1995). Lobe deposits in the lower fan environment are simplified into sub-environments that, from proximal to distal (or more axial to off-axis), include lobe axis, lobe off-axis, lobe fringe, and distal lobe fringe (Fig. 3).

Facies Association descriptions

Facies Association 1 (FA1) is composed of the coarsest-grained facies with the highest proportion of sandstone observed in the Brak River Formation. Although this facies association is dominated by thick sandstone beds of SF1 and SF2 (Fig. 11), it also consists of interbedded SF3 beds and subordinate SF4 beds that are commonly observed between SF1 beds, or at the top of a designated FA1 package. SF5 and SF6 are not present in FA1 and mudstone is rarely preserved.

Facies Association 2 (FA2) comprises a range of sedimentary facies but is overall sandstone-dominated and characterized by sandstone beds

Fig. 11. Representative examples of the four facies associations (FA) identified in the Brak River Formation. Sedimentary facies (SF) commonly observed in each facies association are provided in coloured columns to the left of each example section. Refer to the text for descriptions and interpretations. Internal divisions of low-density (T_a–T_e) and high-density (S_1–S_3) sediment gravity flow deposits are provided to the right of each section and correspond to those assigned by Bouma (1962) and Lowe (1982), respectively.

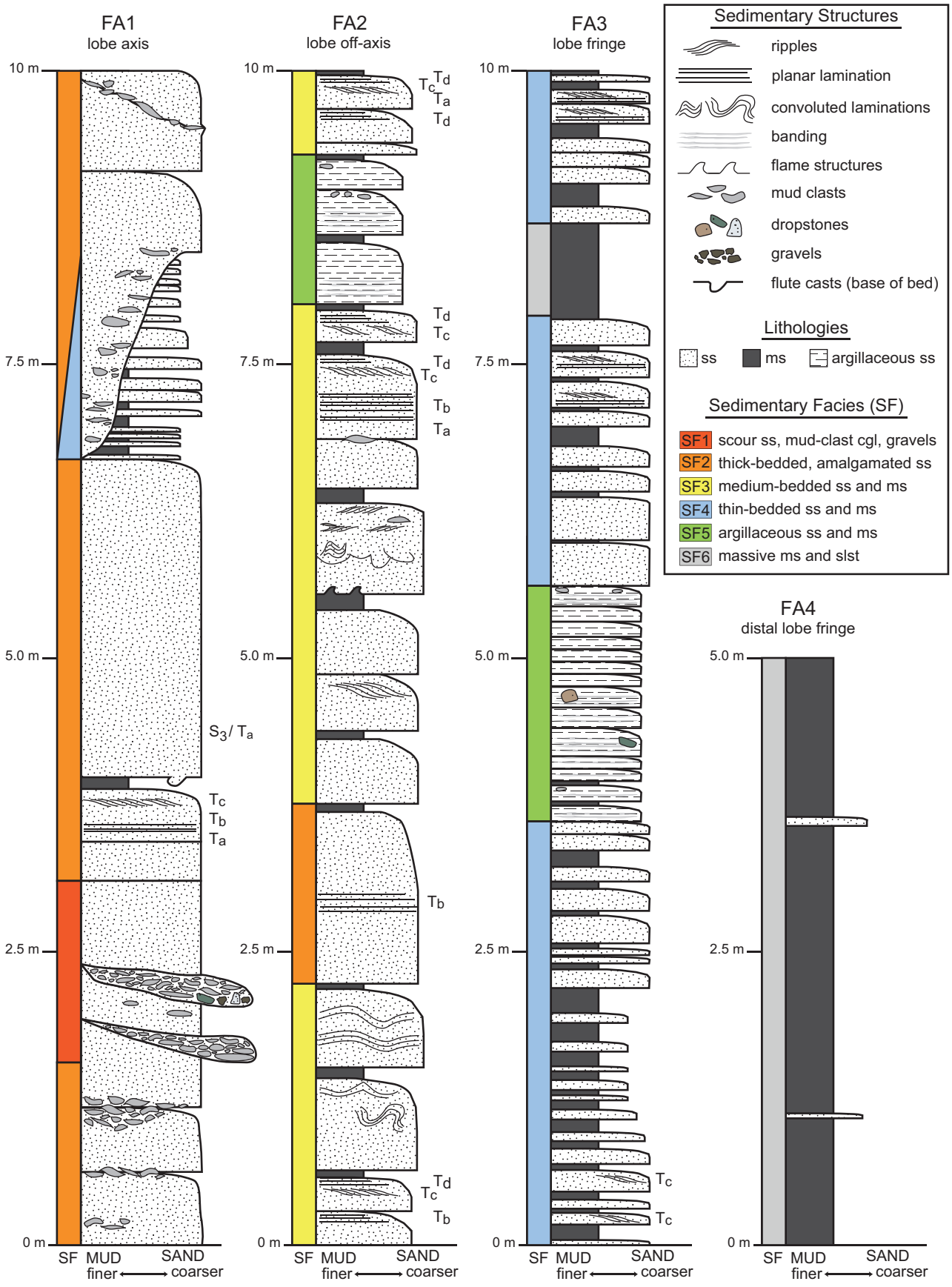

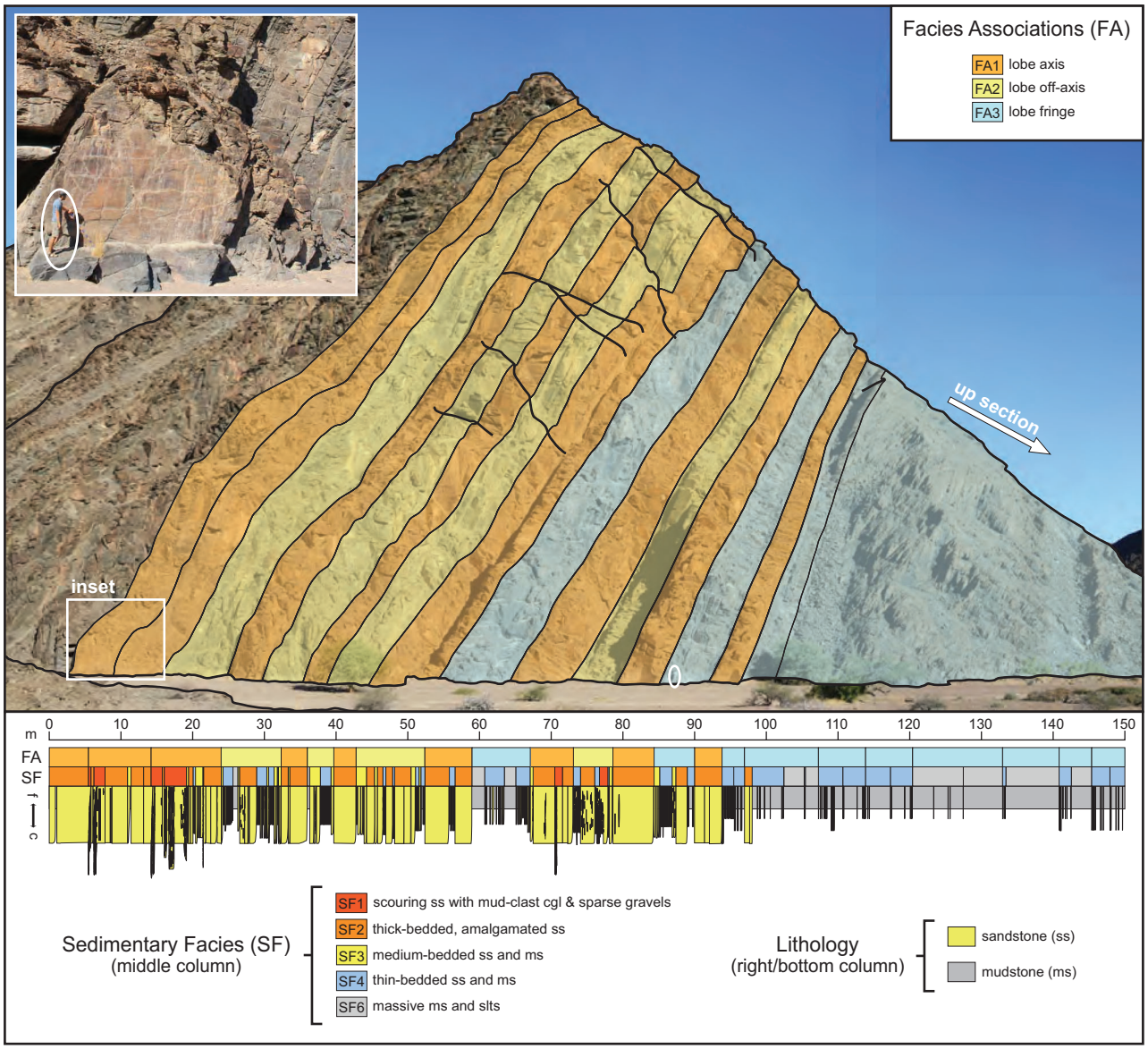

Fig. 12. Partial stratigraphic (uppermost Tinter) section of the upper Brak River Formation (refer to Fig. 5 for full measured section and location), highlighting character of three of the four facies associations (FA) most commonly observed. Facies associations (FA1, FA2, and FA3) have been traced and highlighted on the outcrop image. Person (*ca* 1.8 m tall) standing in front of the outcrop is circled for scale. Inset photograph shows the nature of the outcrop and its exposure at the Tinter section. The uppermost 150 m of stratigraphic section depicted is rotated and provided below the outcrop image with facies associations (FA) in the left/upper column, sedimentary facies (SF) in the middle column, and lithology, with fine-grained (f) to coarse-grained (c) scale, in the right, or bottom column. Note that FA4 and SF5 are not present in this partial section, and thus are not included.

with mudstone caps that are preserved (Fig. 11). SF2 and SF3 are the dominant sedimentary facies of FA2, with subordinate SF4, SF5, and SF6.

Facies Association 3 (FA3) comprises predominantly SF4 and SF6, with relatively minor occurrences of SF5, SF3, and rare SF2 beds.

Facies Association 4 (FA4) is primarily composed of SF6 that is typically tens of metres in thickness, with only minor occurrences of thin sandstone beds (Fig. 11). Although FA4 is relatively thick where present (i.e. 20 to 50 m of uninterrupted mudstone), its original thicknesses have likely been severely affected by tectonic strain and actual thicknesses are uncertain. FA4 tends to be very laterally continuous at a semi-regional scale and is used for

Table 4. Percent sandstone in the Brak River Formation (for each measured stratigraphic section).

Brak River Formation		Adderback		Temple		Petroglyph		Koppie	
Upper	upper mudstone	67%	–	71%	3%	–	–	43%	0%
	upper sandstone		–		79%		–		62%
Middle	middle mudstone	69%	–	–	8%	57%	22%	45%	8%
	middle sandstone		–		–		66%		66%
Lower	lower mudstone	63%	–	–	–	48%	9%	46%	9%
	lower sandstone		–		–		70%		65%
Total		67%	–	–		–		45%	

Petroglyph middle mudstone calculation is partial (overestimated) due to lack of mudstone exposure. Colour shade scale corresponds to low (grey), medium (light yellow), and high (dark yellow) percent sandstone.

correlation within and between structural fold limbs (i.e. Koppie and Temple). FA4 is used to informally break up the Brak River Formation into lower, middle, and upper divisions at Koppie and Temple (Fig. 3).

Facies association interpretations of lobe deposits

Correlation of facies associations and the dominant pattern of lateral and down-dip transitions from FA1 to FA2 to FA3 allow for, and support, interpretations of facies associations representing different lobe sub-environments. All evidence and data from the Zerrissene deep-water system indicate that it is a large (in thickness and lateral extent) and sand-rich fan system, and that lobe deposits are exceptionally sandstone-rich. Thus, FA1 is inferred to represent a lobe axis sub-environment; FA2 is interpreted to represent a lobe off-axis sub-environment; and FA3 is inferred to represent a lobe fringe sub-environment. Relatively thick successions of FA4 are interpreted to have been deposited in an area remote from any confined or distributive sediment source and in a distal lobe fringe portion of the unconfined system in which flows transporting or depositing sand were rare. This sedimentary facies association may represent a basin-plain-like sub-environment that represents the distal expression of sand-carrying flows or it may be indicative of sediment rerouting elsewhere in the basin.

Percent sandstone

Total sandstone percent of the entire Brak River Formation could be calculated only at the Adderback (60%) and Koppie (45%) localities, where the entire thickness was measured (Table 4). Although the covered rocks at the top of the Adderback section, representing about 100 m of strata (Fig. 6), are thought to be dominated by mudstone and thin-bedded sandstone, this interval was excluded because such assumptions greatly impact sandstone percent calculations. All sections at Koppie were used for the total percent sandstone calculation by first totalling the lower, middle, and upper Brak River units, and then normalizing by their average thickness. The sandstone percentages of the lower, middle, and upper Brak River Formation at Koppie are 46%, 45%, and 43%, respectively. Further divisions were calculated for each sand-dominated and mudstone-dominated interval (i.e. lobe complex set) within the lower, middle, and upper Brak River Formation (Table 4; Figs 3 and 4). The sandstone percentages of lower, middle, and upper Brak River Formation are also provided at Adderback – 63%, 69%, and 67%, respectively. Percent sandstone is not divided any further at Adderback due to the lack of significantly thick mudstone-dominated intervals, as are found in Koppie.

Percent sandstone at Temple was calculated as 71% from the three sections measured at that locality and only reflects the uppermost Brak River Formation. Percent sandstone was calculated separately for the Petroglyph section, which only records the lower and middle Brak River Formation, and is comparable to the percent values of the Koppie sections (Table 4). The percent sandstone of the middle mudstone in the Petroglyph section (22%) is partial and likely overestimated because only the lowermost part of this mudstone-dominated interval was exposed and measured.

DISCUSSION

Depositional environment

The Brak River Formation is one of the three siliciclastic intervals of the upper Neoproterozoic Zerrissene Group (Fig. 1C) that represents deep-water

lobe deposits in a large unconfined submarine fan system with possibly the most laterally extensive exposure in the world. Although only the lower fan sub-environment is recorded by the Brak River Formation, it can be inferred that the larger-scale system, including sub-environments that are not preserved, likely represented a very large submarine fan that occupied the north–south-trending and elongate Adamastor Ocean, possibly near the junction of the east–west-trending Khomas Ocean, all between converging Rio de la Plata, Congo, and Kalahari cratons (Miller, 2008; Nieminski *et al.*, 2019).

The lower fan system represented by the Brak River Formation is sandstone dominated, uniformly fine-grained, and has little evidence for highly erosive flows. Sandstone beds and facies of the Brak River Formation are laterally extensive, sheet-like deposits that show little change over distances of many kilometres. Lobe axis, off-axis, and fringe deposits are all represented in the sequence and likely represent basin floor deposition, down-system from any channel-lobe transition zone and without any evidence of major channelization. Coarse-grained deposits are restricted to rare granules–pebbles and extrabasinal clasts from glaciomarine sedimentation (i.e. dropstones).

The lack of coarser-grained material in such a large basin with a thick deep-water succession either signifies that it was far enough from the shelf edge that all coarser material was deposited up-dip and is simply not preserved in the region, or that there was no coarser material available in the source regions. If the latter case were true, and if the source of rare granules–pebbles was not glaciogenic, then the granules–pebbles would reflect a relatively inactive and insignificant source that only periodically contributed coarse material to the ocean basin. Otherwise, it is possible that all of the coarser detritus, granules–pebbles and cobbles, were glaciogenic and dropped into the deep-water system from melting ice cover, and that there was no coarse-grained sediment transfer to the basin. If the overwhelming fine-grained siliciclastic material were a reflection of distal position on the basin floor, then this could also explain the lack of any large erosive features far out in the lower fan environment. When compared with other ancient deep-water lobe depositional systems, the Zerrissene system is remarkably large and sand-rich (for example, Permian Skoorsteenberg Formation of the Karoo Basin and Neoproterozoic Kaza Group of the Windermere Supergroup; Prélat *et al.*, 2009; Terlaky *et al.*, 2016). Although the scale and thickness of each of the architectural orders used to describe the Brak River Formation are comparable to those of systems such as the Skoorsteenberg Formation and Kaza Group, the upper reaches of each of these measures largely exceed them (Table 1) and are likely an indication of greater sediment supply. The collective thickness of deep-water lobe deposits in the Zerrissene Group is another indication of immense sediment supply and may be explained by regional concurrent glacial activity in its related catchment, which has been shown to have implications on drastically increased sediment supply to submarine fan environments (Hessler *et al.*, 2018) and could further explain the overwhelming fine-grained material of the system.

It is notable that studies of other deep-water systems over similar stratigraphic thickness and study area size show systematic transitions from slope to basin floor environments. Whereas deep-water sequences of the Windermere, and of the Tanqua and Laingsburg Karoo, represent many sub-environments of a submarine fan system, including slope-channel complexes and channel-levée environments (Schwarz & Arnott, 2007; Flint *et al.*, 2011), the channel-lobe transition zone (Van der Merwe *et al.*, 2014; Hofstra *et al.*, 2015; Brooks *et al.*, 2018), avulsion and terminal splays (Hodgson *et al.*, 2006; Terlaky & Arnott, 2014; Terlaky *et al.*, 2016), base-of-slope frontal-lobe complexes (Morris *et al.*, 2014), and terminal submarine fan lobes (Prélat *et al.*, 2009; Terlaky *et al.*, 2016), the Zerrissene Group (>1600 m; Swart, 1992) is unique in that it is entirely composed of lower submarine fan depositional environments. Although only the deep-water lobe deposits of the Brak River Formation are described in this study, the underlying Zebraputs and overlying Amis River formations are also interpreted to record the deep-water lobe depositional system (Swart, 1992, 1994; Miller, 2008).

The scale of what are interpreted to represent depositional lobes and the scale at which they are stacked to form lobe complexes, which further assemble into complex sets (Fig. 3), indicate that the length/width scale of lobe complexes was at least in the order of tens of kilometres after a minimum correction due to shortening (*ca* 50%). The lower fan environment of the entire submarine fan system, composed of lobe complex sets, was likely on the order of 100 km wide at a minimum. In its entirety, the Brak River Formation may represent the distal

reaches of a submarine fan system, made up of stacks of lobe complex sets in the lower fan region (Fig. 3). Otherwise, the Brak River Formation may document a very large, fine-grained, and relatively non-erosive frontal lobe deep-water system, and the entirety of the Zerrissene Group may represent the fan system. The lack of full exposure of Zerrissene basin fill and lack of any evidence of submarine channel or canyon makes it difficult to define the larger scale depositional system; the more proximal portions of the Zerrissene system are not exposed or preserved in the Ugab Region.

Erosive surfaces

The occurrence of scours filled with mudstone-clast conglomerate record the highest-energy and most erosive facies documented in the Brak River Formation. The geometry of these scours relative to overall palaeo-transport is not well-constrained. The scours (0.1 to 2.5 m deep, up to 30 m wide) locally observed in SF1 do not document any large-scale channelization. These features are smaller than distal conduits documented in many other deep-water systems (e.g. Twichell *et al.*, 1992; Hodgson *et al.*, 2006). Yet, these smaller-scale scour features may represent poorly defined feeder and distributary conduits to lobes that are increasingly recognized on submarine fans (e.g. Maier *et al.*, 2020; McHargue *et al.*, 2021). Alternatively, if not persisting distributive elements, the scours in the Brak River Formation may reflect the scale of erosional features such as megaflutes. Megaflutes are scours that record localized erosion of the seafloor by energetic, largely bypassing turbidity currents or erosive, unsteady flows (Kane *et al.*, 2009). Megaflutes can occur both in channel-lobe transition zones (e.g. Wynn *et al.*, 2002; Macdonald *et al.*, 2011; Hofstra *et al.*, 2015) and in more medial to distal parts of a lobe (Macdonald *et al.*, 2011). The occurrence of isolated mudstone-clast-filled scours in the Brak River Formation can most often be correlated between stratigraphic sections, suggesting that their associated erosive flows reached at least the kilometre-scale. The Brak River scours are likely not indicative of incipient channel formation, as commonly suggested for megaflutes (Elliott, 2000; Maier *et al.*, 2011; Fildani *et al.*, 2013).

Stratigraphic architecture

Dimensions and geometries of lobe deposits

In the hierarchical scheme defined for the Zerrissene system, correlations of facies associations between the five stratigraphic sections in the Koppie fold limb and the three sections at the Temple locality, provide approximate dimensions and spatial distribution of deep-water lobe deposits (Fig. 3). Although the Zerrissene Group has undergone severe east–west shortening, north–south correlations within the Koppie and Temple fold limbs are not only the most reliable, but also not affected by this major shortening (Fig. 1A). The general palaeoflow interpreted from palaeocurrent data (Fig. 7) suggests that the stratigraphic sections measured in north–south-trending fold limbs (i.e. Koppie 1 to 5 and Temple sections) are near depositional dip sections, whereas correlations made east–west, across fold limbs, transect the basin in an approximate depositional strike direction. Lobe dimensions, as inferred by thickness of facies associations, are typically 2 to 20 m thick and demonstrate a minimum extent of roughly 4 to 10 km in the near dip direction at Temple and Koppie, respectively (Fig. 13). Over this extent, however, changes between lobe axis, off-axis, or lobe fringe are usually observed (i.e. rarely does a lobe axis deposit meet or exceed those dimensions). Lateral transitions from lobe axis, to off-axis, to fringe occur over an average distance of 6 km.

Vertical stacking of lobe deposits

At Koppie, even though the percent sandstone is comparable for lower, middle, and upper Brak River Formation (Table 4), there is more variability documented in the vertical stacking of lobe deposits in the middle and upper Brak River Formation, compared to lower (Fig. 4). Where lobe deposits tend to stack vertically, lobe axis deposits (i.e. FA1) are more commonly observed to stack than lobe off-axis and fringe deposits. Wherever FA1 is stacked, it directly overlies and is directly overlain by lobe fringe deposits (i.e. FA3; Fig. 4). Juxtaposition of more proximal/axial facies associations (i.e. FA1), immediately overlying distal/off-axis facies associations (i.e. FA3) suggests a lateral shift in lobe positions through time. Furthermore, frequent and repeated stratigraphic changes from lobe axis to lobe fringe are inferred to indicate compensational stacking as a driving mechanism of lobe movement, in which the depositional axis of the unconfined flows autogenically avulses to adjust for minor topographic relief caused by the preceding depositing event (Mutti & Sonnino, 1981; Prélat & Hodgson, 2013). However, other controls on spatial positioning of lobe deposits likely occur. For example, FA1 never

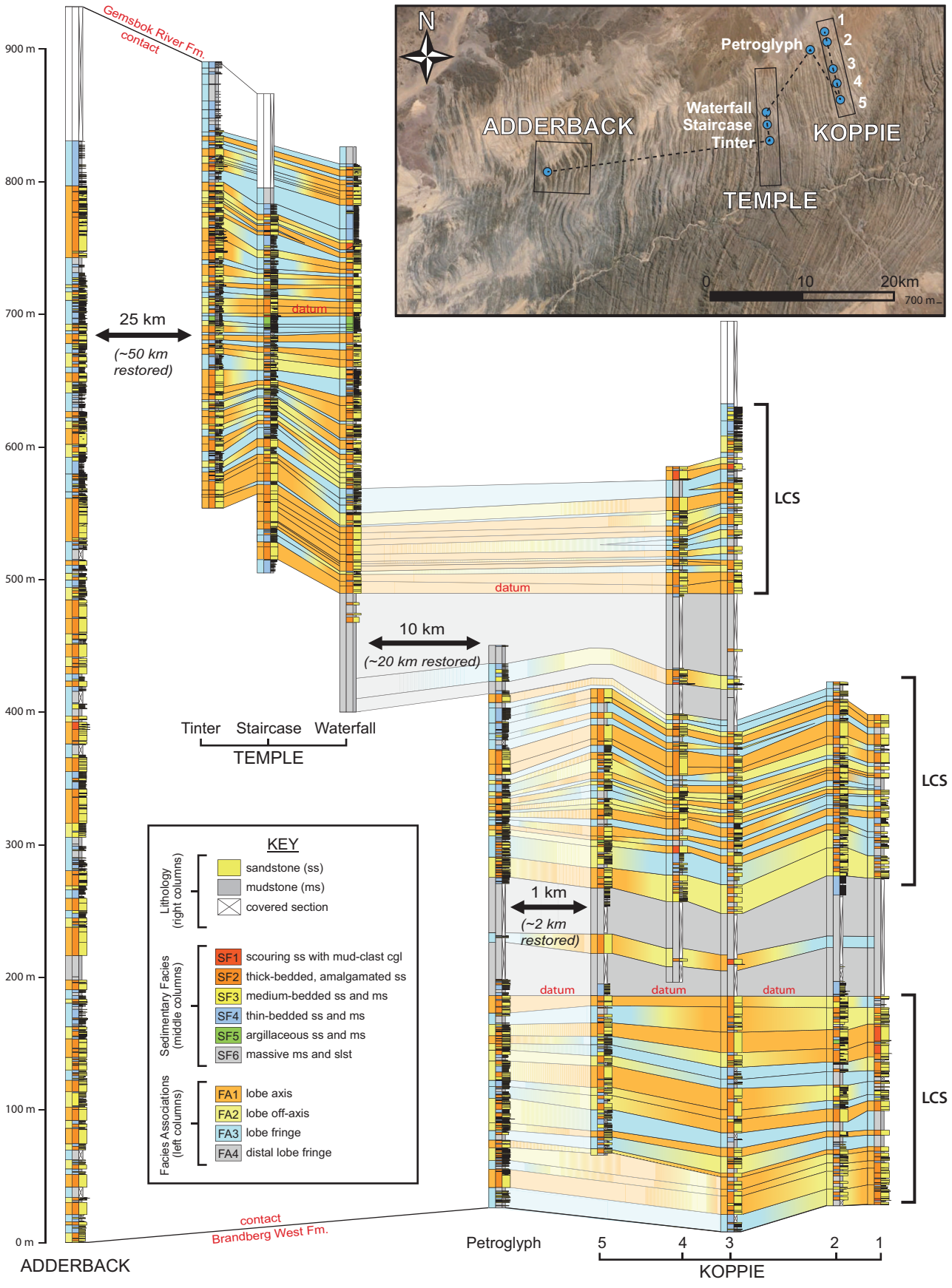

Fig. 13. Ten stratigraphic sections correlated across the basin. Cross-section of correlations is provided on the reference map in the upper right. Gradient colours between correlation lines represent facies associations (FA), or lobe deposits, and their transitions between stratigraphic sections. Solid colour gradients highlight where correlations were mapped within individual fold limbs. Transparent gradient colours show correlations that were interpolated across the basin and geographic distances are provided. Italicized distances between correlated sections account for regional east–west tectonic shortening (estimated minimum *ca* 50%). No correlations or gradients are shown between Adderback and Temple because the distance between these areas exceeds any reasonable measure of lobe deposits represented by correlated facies associations. LCS, lobe complex set.

exceeds five vertically stacked occurrences, but rather moves laterally to directly overlie FA3. In several instances, irregularity of lobe geomorphology may also be documented. Patterns of amalgamation exist over 2 to 4 km and are recognized by the lateral removal of a lower energy facies association between two higher energy facies associations within the same lobe deposit (for example, FA1 to FA2 to FA1).

At least two or three lobe deposits of the same facies association continually stack on top of one another in lower Brak River Formation, whereas abrupt stratigraphic facies changes in lobe facies are more frequent in the middle and upper Brak Formation. For example, at Koppie, FA1 deposits stack as thick as 45 m in the lower Brak River Formation but only as thick as 18 m in the middle or upper Brak River Formation (Fig. 5). The change in thickness and frequency of lateral avulsion suggests an up-section increase in lateral compensational stacking, which may relate to the evolution of the system and overall basin geometry. The lower Brak River Formation records the initiation of the submarine fan system (directly overlying carbonate; Fig. 1C), when any pre-existing topography that may have existed on the seafloor would have influenced sediment routing, lobe positions, and resulting stacking patterns. As the system developed and the basin depocentre accumulated deep-water sediment, a lower gradient basin floor topography was established, and compensational stacking became a mechanism on spatial positioning of lobe deposits (Marini *et al.*, 2015).

System-scale variations

At the eastern (Koppie) locality, the informal lower, middle, and upper divisions of the Brak River Formation each represent a sand-rich lobe complex set that is bound by 60 to 100 m thick mudstone-dominated intervals (Figs 3 and 4). However, the only thick FA4 interval to the west (at Adderback) is <20 m thick and potentially correlates to the lower mudstone-dominated interval at Petroglyph and Koppie (Fig. 13). Instead, this study interprets approximately five sand-rich complex sets at Adderback to the west. An uppermost mudstone-dominated interval below the contact of the Brak River Formation with the overlying Gemsbok River Formation carbonate is more extensive because it is present at both Koppie and Adderback localities. Key differences between mudstone-dominated intervals within the Brak River Formation and the uppermost interval include: (i) the uppermost interval, where exposed in Tinter section, contains thin sandstone beds throughout (FA3-dominated), whereas the lower mudstone-dominated intervals, documented at Koppie and Temple, show at least a couple >10 m exposures of uninterrupted massive mudstone (FA4); (ii) facies associations gradually grade up-section into the FA3-dominated uppermost interval, whereas, there is an abrupt change from commonly FA1 to FA4 in the lower and middle mudstone-dominated intervals at Koppie; and (iii) the upper interval appears to be regional, whereas the thick lower and middle mudstone-dominated intervals are only present at the Koppie and Temple localities. Given these differences, the two mudstone-dominated bounding intervals present at Temple and Koppie, that are used to divide the formation into lower, middle, and upper Brak River Formation, were interpreted to represent the fringes of lobe complex sets due to lateral shifts (or avulsions) of the axis of the system westward into the basin (Boulesteix *et al.*, 2020). At Koppie, these intervals record times when sand supply was significantly reduced and diverted westward (Fig. 13). Consequently, the stratigraphic record observed at all studied localities can be explained by a minimum of five lobe complex sets (Fig. 14). Conversely, the FA3 interval in the uppermost Brak River Formation represents a basin-wide decrease in energy (or siliciclastic sediment supply) as the system transitions into the overlying carbonate Gemsbok River Formation. The sandstone facies deposited by waning energy flows is interpreted as the last pulse of siliciclastic

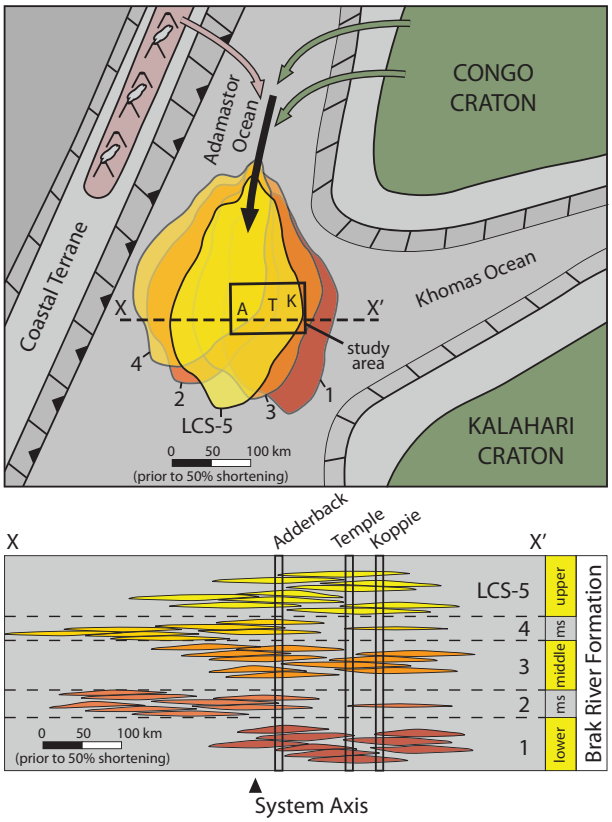

Fig. 14. (Top) Schematic paleogeographic setting of the deep-water Zerrissene basin at the time of deposition of the Brak River Formation, highlighting the hypothetical lateral offset of lobe complex sets (LCS). Study area (black box) was restored to reflect *ca* 50% east–west structural shortening. Sediments were transported (arrows) down a trough-like basin and deposited in an unconfined basin plain at the at junction of the Adamastor and Khomas oceans. The Brak River Formation reflects more axial deep-water lobe deposits in the west and slightly off-axis deposits *ca* 70 km farther east. (Bottom) Chronostratigraphic diagram of the Brak River Formation along X–X' showing hypothetical stacking of the minimum number of LCS to satisfy the stratigraphic relationships observed in the study area. Colours correspond to LCS orientations shown in the above map. A, Adderback locality; K, Koppie locality; T, Temple locality; ms, mudstone-dominated interval.

sedimentation before the establishment of a widespread carbonate platform on the shelf (Miller *et al.*, 2009) that subdued siliciclastic sediment derived from the African continent.

Basin configuration

Provenance analysis suggests that Zerrissene sediments were derived primarily from the north to north-east (Nieminski *et al.*, 2019), which largely agrees with palaeocurrent data presented in this study (Fig. 7) and previously reported palaeocurrent data (Miller *et al.*, 1983a; Swart, 1992; Paciullo *et al.*, 2007). Specifically, Nieminski *et al.* (2019) inferred from detrital zircon U–Pb geochronology that the Congo Craton and East African Orogen to the north–north-east were the primary sources of siliciclastic sediment into the basin, with increasing contribution from the Punta del Este–Coastal Terrane magmatic arc to the west–north-west throughout the deposition of the Zerrissene Group. Detailed study of the Brak River Formation not only supports this sediment source direction, but also allows the authors to make inferences on the basin's relative orientation and shape. Facies patterns, thickness variations, and palaeocurrents all support a general north to south sediment routing, but with significant changes recorded in the deposits from east to west. The Brak River Formation thickens (*ca* 200 m) westward and increases in total sandstone percent from the Koppie to the Adderback locality (Table 4; Fig. 13). Given the interpreted southward sediment transport direction, the western part of the basin was interpreted to represent a more axial position, as opposed to a more proximal location in the fan system. Additionally, the absence of the two 60 to 90 m thick mudstone-dominated intervals at Adderback (interpreted at Koppie and Temple as lobe complex set fringes) and the abundance of thick-bedded sandstone (SF2) throughout the section further supports the interpretation that the farther western section occupied the more axial part of the system in which sand input continuously persisted throughout deposition of the Brak River Formation, regardless of fan orientation within the basin. While the east–west correlations of lobe complex sets reveal lateral shifts in the submarine fan across the basin floor, the authors interpret that persistent lower fan facies throughout the entirety of the Brak River Formation suggests that the north–south position of the Brak River system was relatively stable. It is interpreted herein that the Zerrissene basin was a north–south-oriented deep-water, trough-like basin, generally between South America and Africa (Fig. 14). The Zerrissene Group records large fan systems that are interpreted to have been axially transported down the Adamastor Ocean and deposited within an unconfined basin plain at the junction with the Khomas Ocean.

Conceptual model for sand-rich lobe-dominated submarine fans with rare channelization

McHargue *et al.* (2021) compared seismic facies of deep-water lobe deposits with both pervasive and no apparent channelization and presented a model that related fan architecture to mud content and runout distance of average turbidity currents. Mud-rich turbidite systems, such as the Nile, Congo, and Amazon fans, are dominated by levée-confined channels that distribute sediment throughout the fan and terminate in lobes. Conversely, mud-poor turbidite systems result in erosional confinement (for example, channels and gullies) in proximal areas and sand-rich lobe-dominated fans with scour features but no apparent distributary channels in the distal areas of the system. In the mud-poor continental slope of the Niger Delta, McHargue *et al.* (2021) invoked littoral drift as a mechanism for sorting mud out of the system to suppress the construction of levée confined channels. The modern Mississippi Fan, on the other hand, shows lobes with little channelization dominated by silt-rich strata (Fildani *et al.*, 2018b). In contrast, the thick sand-rich Brak River Formation is almost entirely dominated by lobes deposited in the absence of either erosional or constructional confinement. The Neoproterozoic Brak River Formation submarine fan system can be explained by a conceptual model in which grain-size distribution is strongly controlled by a combination of: (i) voluminous fine-grained sand and silt supplied from glacially modified landscapes (for example, late Pleistocene Mississippi catchment; Hessler *et al.*, 2018); and (ii) long transport distances that sequestered both coarser-grained material and mud upstream in more proximal depositional environments (for example, channel-levée systems). Filtering of sediment by grain size along the depositional system results in turbidity currents with enough mud content to sustain turbulent flow and long runout distances, but not enough to construct levées to support significant channelization.

Although less commonly observed in the Brak River Formation, mud-rich transitional flow deposits likely play a role in maintaining a lobe-dominated system; their abundance in analogous fine-grained laterally extensive deep-water systems with infrequent channelization (for example, modern Mississippi Fan, Fildani *et al.*, 2018b; Unit A of Laingsburg Karoo, Spychala *et al.*, 2017) has been attributed to upstream loss of confinement and erosion at the channel-lobe-transition. Flow expansion and entrainment of finer material from the substrate (silt and clay) into the sediment gravity flow suppresses turbulence (Lowe & Guy, 2000; Haughton *et al.*, 2009) and results in flow stratification with a mud-rich lower boundary layer. Similar flows have been proposed for the Palaeocene Wilcox system (Kane & Pontén, 2012) and seem to be able to travel long distances in modern systems (i.e. Mississippi Fan). Consequently, limited mud content is present in the upper part of the sediment gravity flow and thereby further prevents flow stripping of fine material necessary for construction of levées (Piper & Normark, 1983; Traer *et al.*, 2018).

While the deep-water lobes preserved in the Brak River Formation are relatively unconfined and laterally extensive, the large spatial footprint of the submarine fan system fills the basin floor depocentre that is fixed at the junction of two elongate oceans (i.e. Adamastor and Khomas; Fig. 14). This prolonged deposition drives subsidence and suppressed evident progradation of the fan system.

CONCLUSIONS

The quasi-three-dimensional exposure of the upper Neoproterozoic Zerrissene Group and Brak River Formation documents an extensive, sand-rich submarine fan system with the following findings:

- The Brak River Formation is the middle of three unconfined siliciclastic submarine fan systems that comprise the Zerrissene Group and is dominated by sand-rich lobe deposits.
- The six sedimentary facies recognized in the Brak River Formation reflect lobe deposition consistent with a lower fan environment with no indication of large-scale scouring or channelization expected in upper fan settings.
- The uniformly fine-grained, largely tabular system records lobe axis, off-axis, and fringe deposits (facies associations) that are approximately 2 to 20 m thick and commonly amalgamate. Significant variability in vertical stacking is observed and interpreted as compensation of lobe deposits. Stacking of lobe deposits was aggradational during the initiation of the Brak River submarine fan system (lower complex set), but compensational stacking increasingly became the dominant driver of lobe architecture

as the basin depocentre accumulated sediment and evolved to a less-confined, lower gradient basin floor.

- Facies patterns, thickness variations, percent sandstone, and palaeocurrents, corroborated by provenance analysis, suggest that Zerrissene sediments were derived primarily from the north to north-east. The Brak River Formation of the western study area (Adderback locality) was located in a more axial submarine fan system setting, as evidenced by continuous deposition of sandstone-rich complex sets. Conversely, the Koppie locality (>70 km east) alternates between axial sandstone-rich and fringe mudstone-dominated complex sets and demarcates the margin architecture of a large submarine fan system.
- The centimetre-scale to basin-scale documentation of these deposits provides a new model for long-distance transport of sand-rich deep-water lobes without pervasive channelization.

ACKNOWLEDGEMENTS

This work would not have been possible without the introduction to the field area and stratigraphy provided by Roger Swart. We gratefully acknowledge Dave Hodgson, Ian Kane, Lilian Navarro, and Jason Flaum for their constructive reviews of this manuscript, and *Sedimentology* Editors Jeff Peakall and Jaco Baas for their additional comments. We thank Bruce Power, Morgan Sullivan, Cai Puigdefabregas, Dominic Armitage, Bill Morris, and Fabien Laugier for early discussions related to this work. This research benefited from field assistance provided by Matt Malkowski and field support offered by Chevron. Primary funding for this research was provided by the industry affiliates of the Stanford Project on Deep-water Depositional Systems (SPODDS). The AAPG Grants-in-Aid Program provided additional financial support for fieldwork and data analysis. The completion of this manuscript was partially funded by the U.S. Geological Survey Coastal and Marine Geology Program and Energy Resources Program. Any use of trade, firm, or product names is for descriptive purposes only and does not imply endorsement by the U.S. Government.

DATA AVAILABILITY STATEMENT

The data that support the findings of this study are openly available in the supplementary material of the article. Any additional queries should be directed to the corresponding author of the article.

REFERENCES

Baas, J.H. (2004) Conditions for formation of massive turbiditic sandstones by primary depositional processes. *Sed. Geol.*, **166**, 293–310.

Baas, J.H., **Best, J.L.** and **Peakall, J.** (2011) Depositional processes, bedform development and hybrid bed formation in rapidly decelerated cohesive (mud–sand) sediment flows. *Sedimentology*, **58**, 1953–1987.

Baker, M.L., **Baas, J.H.**, **Malarkey, J.**, **Jacinto, R.S.**, **Craig, M.J.**, **Kane, I.A.** and **Barker, S.** (2017) The effect of clay type on the properties of cohesive sediment gravity flows and their deposits. *J. Sediment. Res.*, **87**, 1176–1195.

Boger, S.D. and **Miller, J.M.** (2004) Terminal suturing of Gondwana and the onset of the Ross–Delamerian Orogeny: the cause and effect of an Early Cambrian reconfiguration of plate motions. *Earth Planet. Sci. Lett.*, **219**, 35–48.

Boger, S.D., **Wilson, C.J.L.** and **Fanning, C.M.** (2001) Early Paleozoic tectonism within the East Antarctic craton: the final suture between east and west Gondwana? *Geology*, **29**, 463–466.

Boulesteix, K., **Poyatos-Moré, M.**, **Hodgson, D.M.**, **Flint, S.S.** and **Taylor, K.G.** (2020) Fringe or background: characterizing deep-water mudstones beyond the basin-floor fan sandstone pinchout. *J. Sediment. Res.*, **90**, 1678–1705.

Bouma, A.H. (1962) *Sedimentology of some Flysch Deposits: A Graphic Approach to Facies Interpretation*, p. 168. Elsevier Pub. Co., Amsterdam.

Bouma, A.H., **Wickens, H.D.** and **Coleman, J.M.** (1995) Architectural characteristics of fine-grained submarine fans: a model applicable to the Gulf of Mexico. *Gulf Coast Assoc. Geol. Soc. Trans.*, **45**, 71–75.

Brooks, H.L., **Hodgson, D.M.**, **Brunt, R.L.**, **Peakall, J.**, **Hofstra, M.** and **Flint, S.S.** (2018) Deep-water channel-lobe transition zone dynamics: processes and depositional architecture, an example from the Karoo Basin, South Africa. *GSA Bull.*, **130**, 1723–1746.

Cardozo, N. and **Allmendinger, R.W.** (2013) Spherical projections with OSXStereonet. *Comput. Geosci.*, **51**, 193–205.

Carvajal, C., **Paull, C.K.**, **Caress, D.W.**, **Fildani, A.**, **Lundsten, E.**, **Anderson, K.**, **Maier, K.L.**, **McGann, M.**, **Gwiazda, R.** and **Herguera, J.C.** (2017) Unraveling the channel–lobe transition zone with high-resolution AUV bathymetry: Navy Fan, offshore Baja California, Mexico. *J. Sed. Res.*, **87**, 1049–1059.

Chapin, M. (1998) Using turbidite outcrop data to influence deepwater development decisions. Geoscience 98, EAGE/AAPG 3rd Research Symposium: Developing and Managing Turbidite Reservoirs, Abstracts, p. 7.

Clift, P.D., **Hodges, K.V.**, **Heslop, D.**, **Hannigan, R.**, **Van Long, H.** and **Calves, G.** (2008) Correlation of Himalayan exhumation rates and Asian monsoon intensity. *Nat. Geosci.*, **1**, 875–880.

Covault, J.A., **Normark, W.R.**, **Romans, B.W.** and **Graham, S.A.** (2007) Highstand fans in the California borderland: the overlooked deep-water depositional systems. *Geology*, **35**, 783–786.

Coward, M.P. (1981) The junction between Pan African Mobile belts in Namibia: its structural history. *Tectonophysics*, **76**, 59–73.

Elliott, T. (2000) Megaflute erosion surfaces and the initiation of turbidite channels. *Geology*, **28**, 119–122.

Fildani, A., **Hubbard, S.M.**, **Covault, J.A.**, **Maier, K.L.**, **Romans, B.W.**, **Traer, M.** and **Rowland, J.C.** (2013) Erosion at inception of deep-sea channels. *Mar. Petrol. Geol.*, **41**, 48–61.

Fildani, A., **Clark, J.**, **Covault, J.A.**, **Power, B.**, **Romans, B.W.** and **Aiello, I.W.** (2018a) Muddy sand and sandy mud on the distal Mississippi fan: implications for lobe depositional processes. *Geosphere*, **14**, 1051–1066.

Fildani, A., **Hessler, A.M.**, **Mason, C.C.**, **McKay, M.P.** and **Stockli, D.F.** (2018b) Late Pleistocene glacial transitions in North America altered major river drainages, as revealed by deep-sea sediment. *Sci. Rep.*, **8**, 1–8.

Flint, S.A., **Hodgson, D.M.**, **Sprague, A.R.**, **Brunt, R.L.**, **Van der Merwe, W.C.**, **Figueiredo, J.**, **Prélat, A.**, **Box, D.**, **Di Celma, C.** and **Kavanagh, J.P.** (2011) Depositional architecture and sequence stratigraphy of the Karoo basin floor to shelf edge succession, Laingsburg depocentre, South Africa. *Mar. Petrol. Geol.*, **28**, 658–674.

Freyer, E.E. and **Hälbich, I.W.** (1994) Deformation history of the lower Ugab Belt. Proterozoic crustal and metallogenic evolution: Abstracts of Geological Society and Geological Survey of Namibia, v. **18**, p. 18.

Frimmel, H.E., **Klötzli, U.S.** and **Siegfried, P.R.** (1996) New Pb-Pb single zircon age constraints on the timing of Neoproterozoic glaciation and continental break-up in Namibia. *J. Geol.*, **98**, 176–190.

Ghosh, B. and **Lowe, D.R.** (1993) *The Architecture of Deep-Water Channel Complexes*. Cretaceous Venado Sandstone Member, Sacramento Valley, California.

Goldfinger, C., **Nelson, C.H.**, **Johnson, J.E.** and **Shipboard Scientific Party** (2003) Holocene earthquake records from the Cascadia subduction zone and northern San Andreas fault based on precise dating of offshore turbidites. *Annu. Rev. Earth Planet. Sci.*, **31**, 555–577.

Goldstein, A., Jr. and **Reno, D.H.** (1952) Petrography and metamorphism of sediments of Ouachita facies. *AAPG Bull.*, **36**, 2275–2290.

Gooley, J.T., **Sharman, G.R.** and **Graham, S.A.** (2021) Reconciling along-strike disparity in slip displacement of the San Andreas fault, central California, USA. *Bulletin*, **133**, 1441–1464.

Goscombe, B.D., **Hand, M.** and **Gray, D.** (2003) Structure of the Kaoko Belt, Namibia: progressive evolution of a classic transpressional orogen. *J. Struct. Geol.*, **25**, 1049–1081.

Gray, D.R., **Foster, D.A.**, **Goscombe, B.**, **Passchier, C.W.** and **Trouw, R.A.** (2006) 40Ar/39Ar thermochronology of the Pan-African Damara Orogen, Namibia, with implications for tectonothermal and geodynamic evolution. *Precambrian Res.*, **150**, 49–72.

Gray, D.R., **Foster, D.A.**, **Meert, J.G.**, **Goscombe, B.D.**, **Armstrong, R.**, **Trouw, R.A.** and **Passchier, C.W.** (2008) A Damara orogen perspective on the assembly of southwestern Gondwana. *Geol. Soc. Lond. Spec. Publ.*, **294**, 257–278.

Halverson, G.P., **Hoffman, P.F.**, **Schrag, D.P.**, **Maloof, A.C.** and **Rice, A.H.N.** (2005) Toward a Neoproterozoic composite carbon-isotope record. *Geol. Soc. Am. Bull.*, **117**, 1181–1207.

Halverson, G.P., **Dudás, F.Ö.**, **Maloof, A.C.** and **Bowring, S.A.** (2007) Evolution of the $^{87}Sr/^{86}Sr$ composition of Neoproterozoic seawater. *Palaeogeogr. Palaeoclimatol. Palaeoecol.*, **256**, 103–129.

Haughton, P., **Davis, C.**, **McCaffrey, W.** and **Barker, S.** (2009) Hybrid sediment gravity flow deposits–classification, origin and significance. *Mar. Petrol. Geol.*, **26**, 1900–1918.

Hessler, A.M. and **Fildani, A.** (2019) Deep-sea fans: tapping into Earth's changing landscapes. *J. Sediment. Res.*, **89**, 1171–1179.

Hessler, A.M., **Covault, J.A.**, **Stockli, D.F.** and **Fildani, A.** (2018) Late Cenozoic cooling favored glacial over tectonic controls on sediment supply to the western Gulf of Mexico. *Geology*, **46**, 995–998.

Hodgson, D.M. (2009) Distribution and origin of hybrid beds in sand-rich submarine fans of the Tanqua depocentre, Karoo Basin, South Africa. *Mar. Petrol. Geol.*, **26**, 1940–1956.

Hodgson, D.M., **Flint, S.S.**, **Hodgetts, D.**, **Drinkwater, N.J.**, **Johannessen, E.P.** and **Luthi, S.M.** (2006) Stratigraphic evolution of fine-grained submarine fan systems, Tanqua depocenter, Karoo Basin, South Africa. *J. Sediment. Res.*, **76**, 20–40.

Hoffman, P.F., **Swart, R.**, **Eckhardt, E.F.** and **Guowei, H.** (1994) Damara orogen of northwest Namibia. Geological Excursion Guide of the Geological Survey of Namibia, 55 pp.

Hoffman, P.F., **Kaufman, A.J.**, **Halverson, G.P.** and **Schrag, D.P.** (1998) A Neoproterozoic snowball Earth. *Science*, **281**, 1342–1346.

Hofstra, M., **Hodgson, D.M.**, **Peakall, J.** and **Flint, S.S.** (2015) Giant scour-fills in ancient channel-lobe transition zones: formative processes and depositional architecture. *Sed. Geol.*, **329**, 98–114.

Jeppe, J.F.B. (1952) The Geology of the Area along the Ugab River, West of Brandberg. Ph.D. thesis, University of Witewatersrand, Johannesburg, 224 pp.

Kane, I.A. and **Fildani, A.** (2021) Anthropogenic pollution in deep-marine sedimentary systems—a geological perspective on the plastic problem. *Geology*, **49**, 607–608.

Kane, I.A. and **Pontén, A.S.** (2012) Submarine transitional flow deposits in the Paleogene Gulf of Mexico. *Geology*, **40**, 1119–1122.

Kane, I.A., **McCaffrey, W.D.** and **Martinsen, O.J.** (2009) Allogenic vs. autogenic controls on megaflute formation. *J. Sediment. Res.*, **79**, 643–651.

Kane, I., **Pontén, A.**, **Vangdal, B.**, **Eggenhuisen, J.**, **Hodgson, D.M.** and **Spychala, Y.T.** (2017) The stratigraphic record and processes of turbidity current transformation across deep-marine lobes. *Sedimentology*, **64**, 1236–1273.

Ketzer, J.M., **Carpentier, B.**, **Le Gallo, Y.** and **Le Thiez, P.** (2005) Geological sequestration of CO2 in mature hydrocarbon fields basin and reservoir numerical modelling of the Forties Field, North Sea. *Oil Gas Sci. Technol.*, **60**, 259–273.

Kneller, B.C. and **Branney, M.J.** (1995) Sustained high-density turbidity currents and the deposition of thick massive sands. *Sedimentology*, **42**, 607–616.

Kneller, B. and **McCaffrey, W.** (1999) Depositional effects of flow nonuniformity and stratification within turbidity currents approaching a bounding slope: deflection, reflection, and facies variation. *J. Sediment. Res.*, **69**, 980–991.

Kneller, B., **Edwards, D.**, **McCaffrey, W.** and **Moore, R.** (1991) Oblique reflection of turbidity currents. *Geology*, **19**, 250–252.

Kukla, P.A. and **Stannistreet, I.G.** (1991) Record of the Damaran Khomas Hochland accretionary prism in central Namibia: refutation of an 'ensialic' origin of a Late Proterozoic orogenic belt. *Geology*, **19**, 473–476.

Lopez, M. (2001) Architecture and depositional pattern of the Quaternary deep-sea fan of the Amazon. *Mar. Petrol. Geol.*, **18**, 479–486.

Lowe, D.R. (1982) Sediment gravity flows: II: depositional models with special reference to the deposits of high density turbidity currents. *J. Sediment. Petrol.*, **52**, 279–297.

Lowe, D.R. and **Guy, M.** (2000) Slurry-flow deposits in the Britannia Formation (Lower Cretaceous), North Sea: a new perspective on the turbidity current and debris flow problem. *Sedimentology*, **47**, 31–70.

Lowe, D.R., **Guy, M.** and **Palfrey, A.** (2003) Facies of slurry-flow deposits: Britannia Formation (Lower Cretaceous), North Sea: implications for flow evolution and deposit geometry. *Sedimentology*, **50**, 45–80.

Lyons, W., **Swart, R.** and **Mohrig, D.** (2007) Deepwater lobes of the Zerrissene Turbidite System, Namibia. In: Nilsen T.H., Shew, R.D., Steffens, G.S. and Studlick, J.R.J., Eds., Atlas of Deep-Water Outcrops: American Association of Petroleum Geologists Studies in Geology **56**, pp. 235–237.

Macdonald, H.A., **Peakall, J.**, **Wignall, P.B.** and **Best, J.** (2011) Sedimentation in deep-sea lobe-elements: implications for the origin of thickening-upward sequences. *J. Geol. Soc. London*, **168**, 319–332.

Maeder, X., **Passchier, C.W.** and **Trouw, R.A.** (2014) Complex vein systems as a data source in tectonics: an example from the Ugab Valley, NW Namibia. *J. Struct. Geol.*, **62**, 125–140.

Maier, K.L., **Fildani, A.**, **Paull, C.K.**, **Graham, S.A.**, **McHargue, T.R.**, **Caress, D.W.** and **McGann, M.** (2011) The elusive character of discontinuous deep-water channels: new insights from Lucia Chica channel system, offshore California. *Geology*, **39**, 327–330.

Maier, K.L., **Paull, C.K.**, **Caress, D.W.**, **Anderson, K.**, **Nieminski, N.M.**, **Lundsten, E.**, **Erwin, B.E.**, **Gwiazda, R.** and **Fildani, A.** (2020) Submarine-fan development revealed by integrated high-resolution datasets from La Jolla Fan, offshore California, USA. *J. Sed. Res.*, **90**, 468–479.

Marini, M., **Milli, S.**, **Ravnås, R.** and **Moscatelli, M.** (2015) A comparative study of confined vs. semi-confined turbidite lobes from the Lower Messinian Laga Basin (Central Apennines, Italy): implications for assessment of reservoir architecture. *Mar. Petrol. Geol.*, **63**, 142–165.

Martinsen, O.J., **Pulham, A.J.**, **Elliott, T.**, **Haughton, P.**, **Pierce, C.**, **Lacchia, A.R.**, **Barker, S.**, **Latre, A.O.**, **Kane, I.**, **Shannon, P.** and **Sevastopulo, G.D.** (2017) Deep-water clastic systems in the Upper Carboniferous (Upper Mississippian–Lower Pennsylvanian) Shannon Basin, western Ireland. *AAPG Bull.*, **101**, 433–439.

Mason, C.C., **Romans, B.W.**, **Stockli, D.F.**, **Mapes, R.W.** and **Fildani, A.** (2019) Detrital zircons reveal sea-level and hydroclimate controls on Amazon River to deep-sea fan sediment transfer. *Geology*, **47**, 563–567.

McHargue, T.R., **Hodgson, D.M.** and **Shelef, E.** (2021) Architectural diversity of submarine lobate deposits. *Front. Earth Sci.*, **9**, 697170.

Meert, J.G. and **Van Der Voo, R.** (1997) The assembly of Gondwana 800-550 Ma. *J. Geodyn.*, **23**, 223–235.

Miller, R.M. (1983) Damara Orogen of South West Africa/Namibia. In: Miller, R.M., Ed., Evolution of the Damara Orogen: Special Publication of the Geological Society of South Africa, **11**, p. 431–515.

Miller, R.M. (2008) *The geology of Namibia, Volume 2, Neoproterozoic to Lower Palaeozoic*, p. 410. Ministry of Mines and Energy, Geological Survey of Namibia, Namibia.

Miller, R.M. and **Schalk, K.E.L.** (1980) Geological map of South West Africa/Namibia (1:1,000,000). Geological Survey of Namibia, Windhoek, 4 sheets.

Miller, R.M., **Freyer, E.E.** and **Hälbich, I.W.** (1983a) A turbidite succession equivalent to the entire Swakop Group. In: Miller, R.M., Ed., Evolution of the Damara Orogen: Special Publication, Geological Society of South Africa, **11**, p. 65–71.

Miller, R.M.G., **Barnes, S.J.** and **Balkwill, G.** (1983b) Possible active margin deposits within the southern Damara Orogen: The Kuiseb Formation between Okahandja and Windhoek. In: Miller, R.M., Ed., Evolution of the Damara Orogen of South West Africa/Namibia: Special Publication of the Geological Society of South Africa, **11**, pp. 73–88.

Miller, R.M., **Frimmel, H.E.** and **Halverson, G.P.** (2009) Ch. 5.3 Passive continental margin evolution. *Dev. Precambrian Geol.*, **16**, 161–181.

Morris, E.A., **Hodgson, D.M.**, **Flint, S.S.**, **Brunt, R.L.**, **Butterworth, P.J.** and **Verhaeghe, J.** (2014) Sedimentology, stratigraphic architecture, and depositional context of submarine frontal-lobe complexes. *J. Sediment. Res.*, **84**, 763–780.

Mulder, T. and **Etienne, S.** (2010) Lobes in deep-sea turbidite systems: state of the art. *Sed. Geol.*, **229**, 75–80.

Mutti, E. and **Sonnino, M.** (1981) Compensation cycles: a diagnostic feature of turbidite sandstone lobes. International Association of Sedimentologists 2nd European Regional Meeting, Bologna, Italy, p. 120–123.

Nieminski, N.M., **Grove, M.** and **Lowe, D.R.** (2019) Provenance of the Neoproterozoic deep-water Zerrissene Group of the Damara Orogen, Namibia, and paleogeographic implications for the closing of the Adamastor Ocean and assembly of the Gondwana supercontinent. *GSA Bull.*, **131**, 355–371.

Paciullo, F.V.P., **Ribeiro, A.**, **Trouw, R.A.J.** and **Passchier, C.W.** (2007) Facies and facies association of the siliciclastic Brak River and carbonate Gemsbok formations in the Lower Ugab River valley, Namibia, W. Africa. *J. Afr. Earth Sci.*, **47**, 121–134.

Peakall, J., **Best, J.**, **Baas, J.H.**, **Hodgson, D.M.**, **Clare, M.A.**, **Talling, P.J.**, **Dorrell, R.M.** and **Lee, D.R.** (2020) An integrated process-based model of flutes and tool marks in deep-water environments: implications for palaeohydraulics, the Bouma sequence and hybrid event beds. *Sedimentology*, **67**, 1601–1666.

Piper, D.W. and **Normark, W.R.** (1983) Turbidite depositional patterns and flow characteristics, Navy Submarine Fan, California Borderland. *Sedimentology*, **30**, 681–694.

Polonia, A., **Nelson, C.H.**, **Romano, S.**, **Vaiani, S.C.**, **Colizza, E.**, **Gasparotto, G.** and **Gasperini, L.** (2017) A depositional model for seismo-turbidites in confined basins based on Ionian Sea deposits. *Mar. Geol.*, **384**, 177–198.

Porada, H. and **Wittig, R.** (1983) Turbidites and their significance for the geosynclinal evolution of the Damara Orogen, South West Africa, Namibia. *Spec. Publ. Geol. Soc. S Afr.*, **11**, 21–36.

Power, B., **Covault, J.**, **Fildani, A.**, **Sullivan, M.**, **Clark, J.**, **Carson, B.**, **Zarra, L.** and **Romans, B.** (2013) Facies analysis and interpretation of argillaceous sandstone beds in the Paleogene Wilcox Formation, deepwater Gulf of Mexico. *Gulf Coast Assoc. Geol. Soc. Trans.*, **63**, 575–578.

Prave, A.R. (1996) Tale of three cratons: tectonostratigraphic anatomy of the Damara Orogen in northwestern Namibia and the assembly of Gondwana. *Geology*, **24**, 1115–1118.

Prélat, A. and **Hodgson, D.M.** (2013) The full range of turbidite bed thickness patterns in submarine lobes: controls and implications. *J. Geol. Soc. London*, **170**, 209–214.

Prélat, A., **Hodgson, D.M.** and **Flint, S.S.** (2009) Evolution, architecture and hierarchy of distributary deep-water deposits: a high-resolution outcrop investigation from the Permian Karoo Basin, South Africa. *Sedimentology*, **56**, 2132–2154.

Prins, M.A. and **Postma, G.** (2000) Effects of climate, sea level, and tectonics unraveled for last deglaciation turbidite records of the Arabian Sea. *Geology*, **28**, 375–378.

Rapalini, A.E. (2006) New late Proterozoic palaeomagnetic pole for the Rı'o de la Plata Craton: implications for Gondwana. *Precambrian Res.*, **147**, 223–233.

Reading, H.G. and **Richards, M.** (1994) Turbidite systems in deep-water basin margins classified by grain size and feeder system. *AAPG Bull.*, **78**, 792–822.

Schwarz, E. and **Arnott, R.W.C.** (2007) Anatomy and evolution of a slope channel-complex set (Neoproterozoic Isaac Formation, Windermere Supergroup, southern Canadian Cordillera): implications for reservoir characterization. *J. Sediment. Res.*, **77**, 89–109.

Seth, B., **Jung, S.** and **Gruner, B.** (2008) Deciphering polymetamorphic episodes in high-grade metamorphic orogens: constraints from PbSL, Sm/Nd and Lu/Hf garnet dating of low-to high-grade metasedimentary rocks from the Kaoko Belt (Namibia). *Lithostratigraphy*, **104**, 131–146.

Shanmugam, G. (1996) High-density turbidity currents: are they sandy debris flows?: perspectives. *J. Sediment. Res.*, **66**, 2–10.

Sharman, G.R., **Graham, S.A.**, **Grove, M.** and **Hourigan, J.K.** (2013) A reappraisal of the early slip history of the San Andreas fault, central California, USA. *Geology*, **41**, 727–730.

Sharman, G.R., **Covault, J.A.**, **Stockli, D.F.**, **Wroblewski, A.F.J.** and **Bush, M.A.** (2017) Early Cenozoic drainage reorganization of the United States Western Interior–Gulf of Mexico sediment routing system. *Geology*, **45**, 187–190.

Sinclair, H.D. (1994) The influence of lateral basinal slopes on turbidite sedimentation in the Annot sandstones of SE France. *J. Sediment. Res.*, **64**, 42–54.

Spychala, Y.T., **Hodgson, D.M.** and **Lee, D.R.** (2017) Autogenic controls on hybrid bed distribution in submarine lobe complexes. *Mar. Petrol. Geol.*, **88**, 1078–1093.

Stevenson, C.J., **Peakall, J.**, **Hodgson, D.M.**, **Bell, D.** and **Privat, A.** (2020) TB or not TB: banding in turbidite sandstones. *J. Sediment. Res.*, **90**, 821–842.

Stow, D.A. and **Johansson, M.** (2000) Deep-water massive sands: nature, origin and hydrocarbon implications. *Mar. Petrol. Geol.*, **17**, 145–174.

Swart, R. (1992) The sedimentology of the Zerrissene turbidite system, Damara Orogen, Namibia. *Geol. Surv. Namibia Mem.*, **13**, 54.

Swart, R. (1994) Late precambrian outer-fan turbidites from Namibia – vertical and lateral characteristics. *J. Afr. Earth Sci.*, **18**, 3–13.

Talling, P.J. (2013) Hybrid submarine flows comprising turbidity current and cohesive debris flow: deposits, theoretical and experimental analyses, and generalized models. *Geosphere*, **9**, 460–488.

Talling, P.J., **Wynn, R.B.**, **Masson, D.G.**, **Frenz, M.**, **Cronin, B.T.**, **Schiebel, R.**, **Akhmetzhanov, A.M.**, **Dallmeier-Tiessen, S.**, **Benetti, S.**, **Weaver, P.P.E.** and **Georgiopoulou, A.** (2007) Onset of submarine debris flow deposition far from original giant landslide. *Nature*, **450**, 541–544.

Talling, P.J., **Masson, D.G.**, **Sumner, E.J.** and **Malgesini, G.** (2012) Subaqueous sediment density flows: depositional processes and deposit types. *Sedimentology*, **59**, 1937–2003.

Terlaky, V. and **Arnott, R.W.C.** (2014) Matrix-rich and associated matrix-poor sandstones: avulsion splays in slope and basin-floor strata. *Sedimentology*, **61**, 1175–1197.

Terlaky, V., **Rocheleau, J.** and **Arnott, R.W.C.** (2016) Stratal composition and stratigraphic organization of stratal elements in an ancient deep-marine basin-floor succession, Neoproterozoic Windermere Supergroup, British Columbia, Canada. *Sedimentology*, **63**, 136–175.

Tohver, E., **D'Agrella-Filho, M.S.** and **Trindade, R.I.** (2006) Paleomagnetic record of Africa and South America for the 1200–500Ma interval, and evaluation of Rodinia and Gondwana assemblies. *Precambrian Res.*, **147**, 193–222.

Traer, M.M., **Fildani, A.**, **Fringer, O.**, **McHargue, T.R.** and **Hilley, G.E.** (2018) Turbidity current dynamics: 1. Model formulation and identification of flow equilibrium conditions resulting from flow stripping and overspill. *J. Geophys. Res. Earth*, **123, 501–519**.

Twichell, D.C., **Schwab, W.C.**, **Nelson, C.H.**, **Kenyon, N.H.** and **Lee, H.J.** (1992) Characteristics of a sandy depositional lobe on the outer Mississippi fan from SeaMARC IA sidescan sonar images. *Geology*, **20**, 689–692.

Van der Merwe, W.C., **Hodgson, D.M.**, **Brunt, R.L.** and **Flint, S.S.** (2014) Depositional architecture of sand-attached and sand-detached channel-lobe transition zones on an exhumed stepped slope mapped over a 2500 km2 area. *Geosphere*, **10**, 1076–1093.

Weber, M.E., **Wiedicke, M.H.**, **Kudrass, H.R.**, **Hübscher, C.** and **Erlenkeuser, H.** (1997) Active growth of the Bengal Fan during sea-level rise and highstand. *Geology*, **25**, 315–318.

Wynn, R.B., **Kenyon, N.H.**, **Masson, D.G.**, **Stow, D.A.** and **Weaver, P.P.** (2002) Characterization and recognition of deep-water channel-lobe transition zones. *AAPG Bull.*, **86**, 1441–1462.

Zarra, L. (2007) Chronostratigraphic framework for the Wilcox Formation (upper Paleocene–lower Eocene) in the deep-water Gulf of Mexico: Biostratigraphy, sequences, and depositional systems. In: Kennan, L., Pindell, J., Rosen, N., Eds., The Paleogene of the Gulf of Mexico and Caribbean Basins: Processes, Events, and Petroleum Systems: 27th Annual Perkins Research Conference: Gulf Coast Section of the Society for Sedimentary Geology (GCSSEPM) Foundation Publication GCS027, December 2–5, Houston, Texas, pp. 81–145.

Manuscript received 5 July 2022; revision accepted 25 July 2023

Supporting Information

Additional information may be found in the online version of this article:

Appendix S1. Stratigraphic sections Adderback, Temple, and Koppie.

Appendix S2. Stratigraphic sections Windy Wash and Rhino Wash.

Appendix S3. Palaeocurrent measurements and bedding corrections.